AMERICAN SOCIETY FOR MICROBIOLOGY | Molecular and Cellular Biology®

RESEARCH ARTICLE

Meiosis-Specific Functions of Kinesin Motors in Cohesin Removal and Maintenance of Chromosome Integrity in Budding Yeast

Priyanka Mittal,[b] Komal Ghule,[a] Deepika Trakroo,[a] Hemant Kumar Prajapati,[b] Santanu K. Ghosh[a]

[a]Department of Biosciences and Bioengineering, Indian Institute of Technology, Bombay, Powai, Mumbai, India
[b]National Institute of Child Health and Human Development, National Institutes of Health, Bethesda, Maryland, USA

Komal Ghule, Deepika Trakroo, and Hemant Kumar Prajapati contributed equally to this work.

ABSTRACT Kinesin motors provide the molecular forces at the kinetochore-microtubule interface and along the spindle to control chromosome segregation. During meiosis with two rounds of microtubule assembly-disassembly, the roles of motor proteins remain unexplored. We observed that in contrast to mitosis, Cin8 and Kip3 together are indispensable for meiosis. While examining meiosis in *cin8*Δ *kip3*Δ cells, we detected chromosome breakage in the meiosis II cells. The double mutant exhibits a delay in cohesin removal during anaphase I. Consequently, some cells fail to undergo meiosis II and form dyads, while some, as they progress through meiosis II, cause a defect in chromosome integrity. We believe that in the latter cells, an imbalance of spindle-mediated force and the simultaneous persistence of cohesin on chromosomes cause their breakage. We provide evidence that tension generated by Cin8 and Kip3 through microtubule cross-linking is essential for signaling efficient cohesin removal and the maintenance of chromosome integrity during meiosis.

KEYWORDS motor proteins, chromosome segregation, kinetochore, cohesin, meiosis, *S. cerevisiae*

Meiotic chromosome segregation comprises certain unique events distinct from mitosis. In budding yeast, these events include late assembly of the mature kinetochore competent to connect the microtubules, pairing of homologs, mono-orientation of the sister kinetochores with respect to the spindle pole in metaphase I, a stepwise dissolution of cohesin from chromatin, two rounds of chromosome segregation with spindle assembly and disassembly, and partial dephosphorylation of the cyclin-dependent kinase (CDK) substrates adequate for spindle disassembly at meiosis I but not for DNA replication. Furthermore, while dephosphorylation of CDK substrates by Cdc14 phosphatase released by the mitotic exit network (MEN) pathway from its inhibited state is essential for cell cycle exit in both mitosis and meiosis, Cdc14 released by the Cdc14 fourteen early anaphase release (FEAR) pathway appears to be dispensable for the same in mitosis but not in meiosis, as it is required to exit from meiosis I (1–3). Nevertheless, FEAR-dependent Cdc14 release has significant roles in both mitosis and meiosis for coherent segregation of all chromosomal loci and for stability and proper orientation of the microtubule spindle (2, 4–7).

Irrespective of the type of cell cycle, the formation of a microtubule-based spindle and movement of chromosomes along the spindle being attached to the microtubule play a pivotal role during chromosome segregation. The occurrence of these events relies on the polymerization-depolymerization property of the microtubules, which is facilitated by the functions of several microtubule-associated proteins (MAPs) and microtubule-based motors (8). In *Saccharomyces cerevisiae*, four nuclear motors of the

Citation Mittal P, Ghule K, Trakroo D, Prajapati HK, Ghosh SK. 2020. Meiosis-specific functions of kinesin motors in cohesin removal and maintenance of chromosome integrity in budding yeast. Mol Cell Biol 40:e00386-19. https://doi.org/10.1128/MCB.00386-19.

Address correspondence to Santanu K. Ghosh, santanughosh@iitb.ac.in.

Received 17 August 2019
Returned for modification 20 September 2019
Accepted 26 December 2019
Accepted manuscript posted online 21 January 2020
Published 30 March 2020

kinesin superfamily (kinesin-related proteins [KRPs]), namely, Cin8, Kip1, Kip3, and Kar3, have essential roles in chromosome segregation (9–13). However, due to functional redundancy among these motors, they are nonessential for growth (14, 15).

Cin8 and Kip1 belong to the BimC or kinesin-5 family of proteins, where the motor domain is at the amino-terminal end of the protein and motor movement is directed toward the plus end of the microtubule (16, 17). Cin8 and Kip1 form homotetramers, and their plus-end-directed functions are to extend the spindle by pushing the poles apart and to maintain the kinetochores in a clustered form through cross-linking of antiparallel and parallel microtubules, respectively (18–22). Later, through *in vitro* assays, minus-end-directed movement of both single motors has been identified when they work singly on an individual microtubule (23–26). Recently, it has been shown under *in vivo* conditions that Cin8 clusters at the minus end and spindle pole bodies (SPBs) during the early stage of mitosis for capturing the microtubules emanating from opposite SPBs, which facilitates bipolar spindle formation (27). However, the implication of Kip1 minus-end-directed movement has not been explored. In addition to the cross-linking function, Cin8 and, to a lesser extent, Kip1 can also depolymerize kMT (kinetochore-microtubule) in a length-dependent manner, which is believed to be essential for congression of the chromosomes (28). The regulation of Cin8 and Kip1 functions depends on the phosphorylation status of these proteins, where their phosphorylation by Cdk1 during early mitosis mediates SPB separation (29). In metaphase, Cin8 and Kip1 are localized at the centromeres and along the length of the microtubule (13). Since the phosphorylation of Cin8 inhibits its association with the microtubules (30), following the metaphase-to-anaphase transition, dephosphorylation of Cin8 by protein phosphatase 2A regulatory subunit Cdc55 ($PP2A^{Cdc55}$) and Cdc14 phosphatase results in its accumulation near the spindle poles and at the spindle midzone, which is crucial for spindle elongation (31, 32). However, it is not known if a similar dephosphorylation also occurs in Kip1. During early anaphase, anaphase-promoting complex-bound activator protein Cdc20 (APC^{Cdc20}) degrades Kip1 (33), whereas Cin8 is degraded during late anaphase by anaphase-promoting complex-bound activator protein Cdh1 (APC^{Cdh1}) (34). On the other hand, the primary function of the Kip3 motor, belonging to the kinesin-8 family of proteins, is the depolymerization of microtubule plus ends by a mechanism similar to that of kinesin-13 motors (12, 35), which has a role in the movement of chromosomes during anaphase (13, 36). However, Kip3 also slides and clusters the microtubules by cross-linking antiparallel and parallel microtubules, respectively, through its tail domain (37). However, the cross-linking function of Kip3 is trivial compared to kinesin-5 proteins owing to its intrinsic structural ability to form homodimers but not the homotetramers observed in kinesin-5 motors (18–22, 37). Kip3 activity appears to be regulated spatially and temporally based on the length of the spindle and the exact localization of the motor. On a short spindle, it helps in clustering and alignment of the kinetochores by cross-linking of the parallel microtubules and depolymerase activity at the plus ends. During an increase in the spindle length, Kip3 cross-links and slides the antiparallel interpolar microtubules. Finally, when the spindle reaches its maximum length, Kip3 localizes at the plus ends and causes spindle disassembly by its depolymerization activity (22, 38). Kar3 (a minus-end-directed kinesin-14 family protein) is another microtubule depolymerizer present in the cell and is functionally antagonistic to Cin8/Kip1 spindle elongation activity. Kar3 pulls two spindle poles together; therefore, the spindle collapse observed in the absence of both Cin8 and Kip1 can be suppressed by reducing the activity of Kar3 (39). Additionally, Kar3 appears to promote kinetochore-microtubule attachment, as in mitosis, it is found to occupy a subset of kinetochores on which microtubule attachments are slow to form (13).

As described above, several groups have elucidated the functions of nuclear kinesin motors in chromosome segregation in mitosis. Given the mechanistic uniqueness in chromosome segregation in meiosis, as outlined above, it is intriguing to investigate their functions during this cell cycle. However, a *KAR3* mutant was found to be arrested at prophase I (40, 41), which makes it difficult to analyze the meiotic events in the

absence of Kar3. Therefore, in this study, we focused on elucidating the functions of three motors, Cin8, Kip1, and Kip3, in meiosis. Using knockout mutants, we observed that these motors are required for homolog pairing. Strikingly, we noticed that cells with a loss of both Cin8 and Kip3 harbor chromosome breakage. Further investigation argues for a defect in Rec8-cohesin removal from chromatin in these cells. We propose that the conditions in the absence of Cin8 and Kip3 perhaps create an imbalance between the microtubule-mediated force generated by other motors and the resisting force by persistent cohesin, which may lead to chromosome breakage. From our findings, we suggest that the tension generated by the cross-linking activity of Cin8 and Kip3 is crucial to signal cells for cohesin cleavage. Thus, our study reveals significant roles of kinesin motors in meiosis and hints at the essentiality of these proteins in suppressing aneuploidy during gametogenesis.

RESULTS

The motors are required for faithful meiosis. In the first set of experiments, we compared spore viabilities, a readout for faithful meiosis, between the wild type and the individual motor mutants. Given that there are functional redundancies among the motors, we observed a marginal decrease in spore viability in *kip1*Δ and *kip3*Δ mutants (approximately 89 and 92%, respectively). However, the *cin8*Δ mutant showed an ~65% reduction in spore viability, suggesting that this protein is more significant in meiosis (Fig. 1A). It is expected that the pace of meiotic progression can slow down if there is any perturbation in meiosis. To test this, the wild-type and mutant strains were released into synchronized meiosis. Consistent with the spore viability data, we observed that the *cin8*Δ mutant showed a delay at metaphase I compared to the wild type and the *kip1*Δ and *kip3*Δ mutants (Fig. 1Bii), suggesting that some defect is occurring during early meiotic events in the absence of Cin8 and that perhaps, due to functional redundancy, the defect is not apparent in *kip1*Δ and *kip3*Δ mutants. To investigate if the defect causes chromosomes to missegregate, we marked both CenV homologs with the TetO/TetR-green fluorescent protein (GFP) system (see Materials and Methods) and observed their distribution at the end of meiosis. Following faithful meiosis, a tetranucleated cell would show one GFP dot in each nucleus (type I) (Fig. 1D). However, four GFP dots in three and two nuclei (types II and III) or in one nucleus account for chromosome missegregation. Meiotic induction, unless otherwise mentioned, was carried out at 33°C, as the phenotype of the loss of Cin8 becomes aggravated at a higher temperature (13, 42, 43). We observed around 50, 22, and 17% (type II and type III) chromosome missegregation in *cin8*Δ, *kip1*Δ, and *kip3*Δ cells, respectively (Fig. 1D), suggesting that the spore viability defect is probably due to the generation of aneuploidy. As in the *cin8*Δ mutant, the delay in the cell cycle occurs in metaphase I, we presumed that at least some defects might be occurring during the preceding events of chromosome segregation, which include chromatid cohesion, homolog pairing, and sister chromatid mono-orientation. To investigate cohesion between the sisters and the orientation of their spindle attachment, both sisters of one homolog were marked with the TetO/TetR-GFP system. In metaphase I-arrested cells, a defect in sister chromatid mono-orientation would appear as two GFP dots. On the other hand, noncohesed sisters in the cycling cells would produce binucleates with one GFP dot in each nucleus. However, we failed to detect any defect in either sister chromatid mono-orientation or their cohesion (Fig. 2A and B). Although not for Cin8, Kip1, or Kip3, the role of Kar3 in sister chromatid cohesion in mitosis has been reported previously (44).

However, we observed an increased defect in homolog pairing in the *cin8*Δ mutant when both CenV homologs were marked with GFP (type II and type III) (Fig. 2C). Consistent with this, we observed a higher percentage of mislocalization (polycomplex formation) of Zip1, a component of the synaptonemal complex (SC) that reinforces pairing (Fig. 2D). A similar result was also obtained previously, where homologs failed to synapse in the absence of Kar3 (40). Although both the *cin8*Δ and *kip1*Δ mutants showed defects in the localization of Zip1, only *cin8*Δ cells showed a homolog pairing defect. Since Cin8 has a more significant role than Kip1 in mitosis (16) and in meiosis

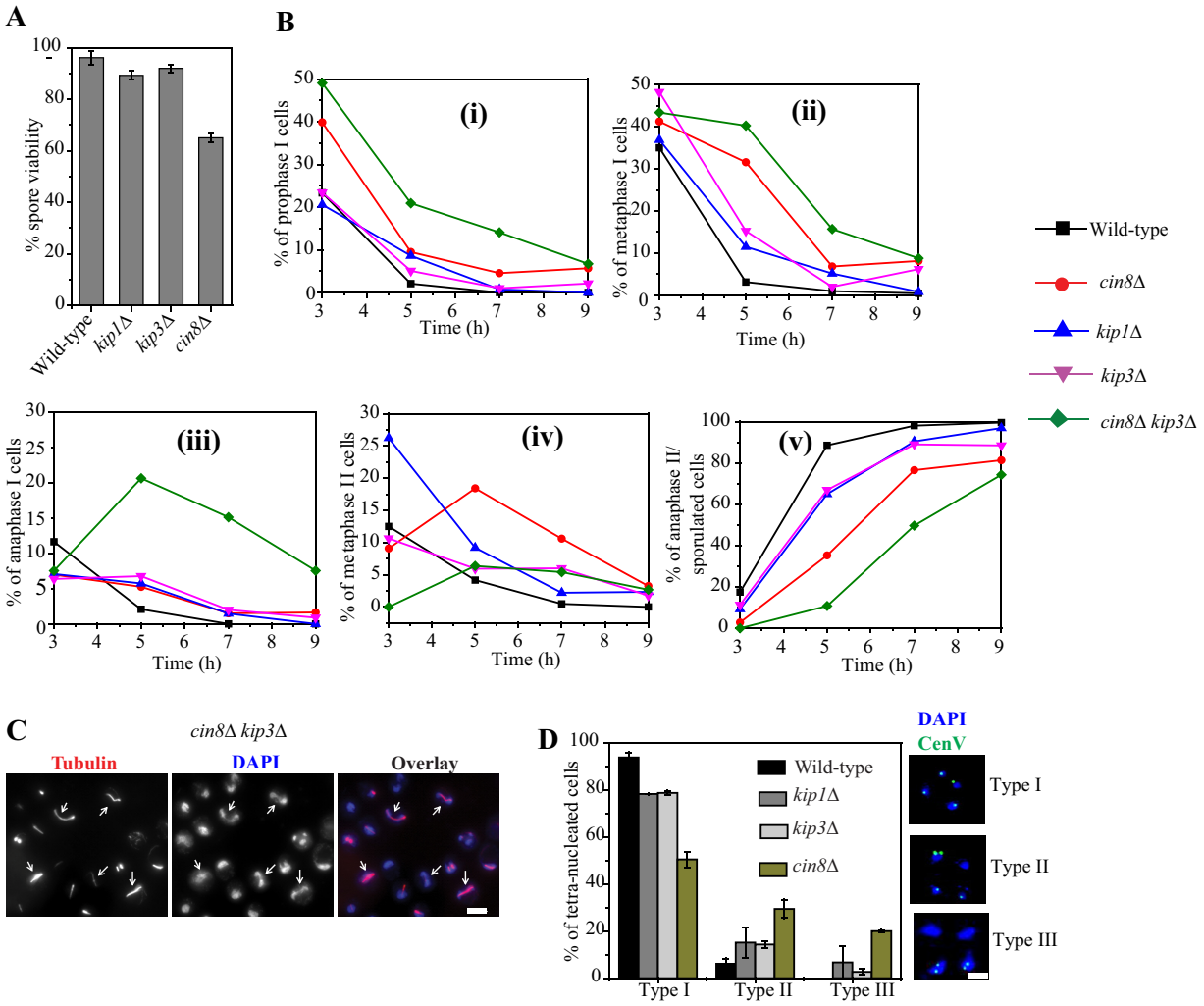

FIG 1 Meiosis in the motor mutants. (A) Spore viabilities of wild-type (SGY5001) ($n = 40$), *cin8*Δ (SGY315) ($n = 60$), *kip1*Δ (SGY317) ($n = 107$), and *kip3*Δ (SGY314) ($n = 91$) cells were analyzed after induction of meiosis at 30°C. "*n*" represents the number of tetrads dissected. (B) The indicated strains were induced for synchronized meiosis and analyzed for meiotic progression. At the indicated time points, the fraction of cells at different stages of meiosis was determined by anti-α-tubulin staining. At least 100 cells were counted for each time point. (C) Representative images of *cin8*Δ *kip3*Δ cells showing the maximum population at the anaphase I stage at 5 h of meiotic induction as determined by anti-α-tubulin and DAPI staining. Arrows indicate anaphase I cells. Bar, 5 μm. (D) The indicated strains harboring homozygous CenV-GFP (see Materials and Methods) were analyzed for meiotic chromosome segregation at 33°C in tetranucleated cells ($n = 90$ to 150). Error bars represent the standard deviations from the mean values obtained from three independent experiments. Bar, 2 μm.

(as shown by spore viability assays) (Fig. 1A), more roles of Cin8 than of Kip1 are expected. Following disassembly of the SC, Zip1 is maintained at the centromeres until the proper bipolar attachment of the homologs is achieved (45). As the Zip1 localization was compromised in the *cin8*Δ or *kip1*Δ mutant, we examined the homolog biorientation of motor mutants where both CenV homologs were marked with GFP. About 37% of the binucleated cells of the *cin8*Δ mutant showed homolog nondisjunction, compared to only 7% in the wild type (type II) (Fig. 2E), while for the *kip3*Δ and *kip1*Δ mutants, the populations exhibiting such a defect were relatively smaller (14% and 11%, respectively) (Fig. 2E). The above-described results suggest that the absence of motor proteins, especially Cin8, can affect homolog pairing in meiosis.

Meiosis is profoundly compromised in the *cin8*Δ *kip3*Δ double mutant. Since Cin8, Kip1, and Kip3 share overlapping functions in microtubule cross-linking and depolymerization (10, 12, 13, 16, 28, 38, 46), we argued that their functions cannot be properly revealed by studying only the single mutants. Therefore, we generated the two only possible viable double mutants, *kip1*Δ *kip3*Δ and *cin8*Δ *kip3*Δ, as the *cin8*Δ

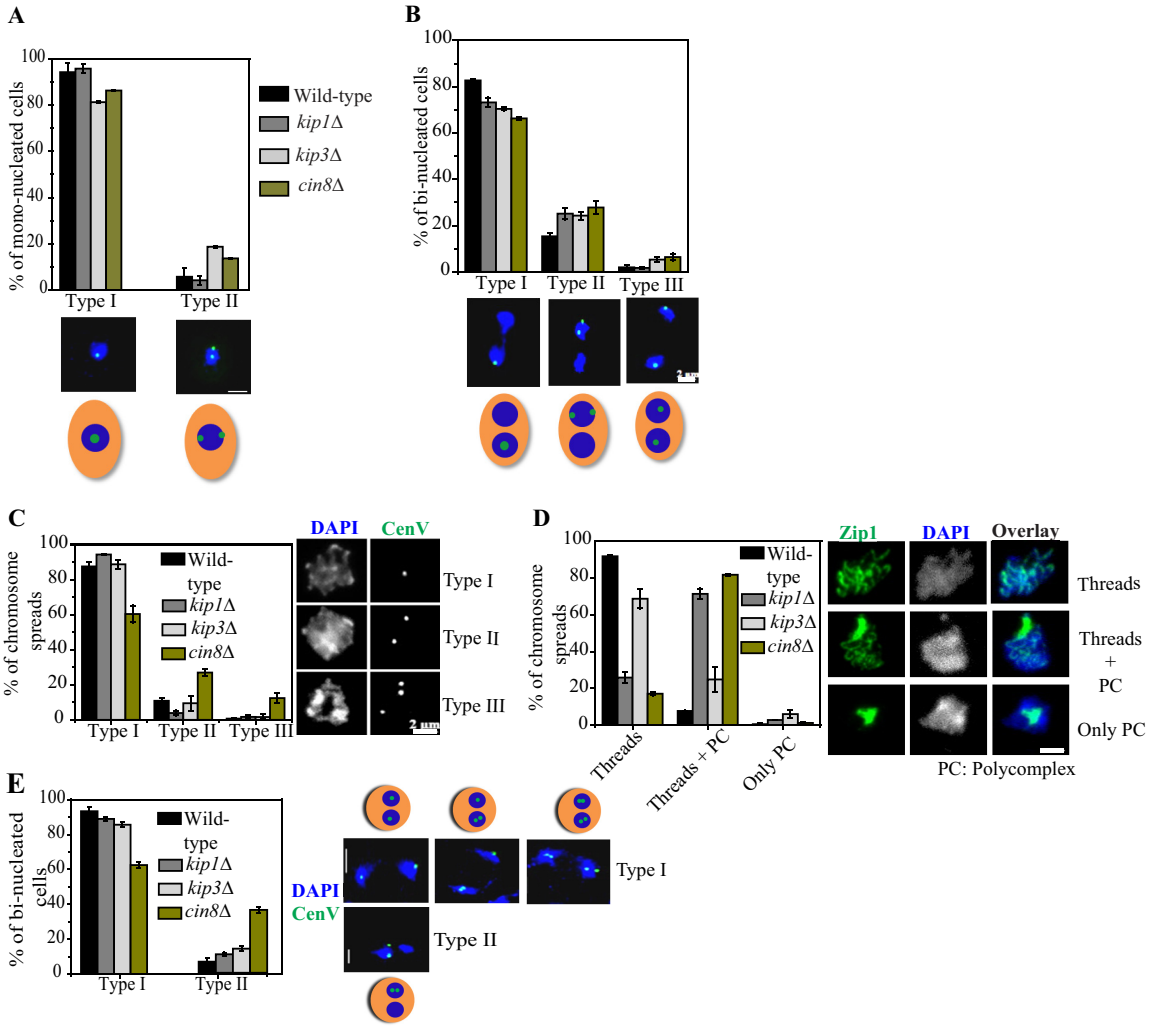

FIG 2 Motor proteins are required for homolog pairing and their disjunction but do not have a role in sister chromatid mono-orientation or cohesion. (A and B) Heterozygously marked CenV-GFP dots were analyzed for meiotic chromosome segregation at 33°C. (A) Metaphase I-arrested wild-type (SGY5143) ($n = 90$), *cin8*Δ (SGY5078) ($n = 124$), *kip1*Δ (SGY5018) ($n = 91$), and *kip3*Δ (SGY5034) ($n = 71$) cells were analyzed for the percentage of mononucleated cells with one or separated sister centromeres ($n = 70$ to 120). (B) Wild-type (SGY5006) ($n = 95$), *cin8*Δ (SGY5090) ($n = 122$), *kip1*Δ (SGY5077) ($n = 97$), and *kip3*Δ (SGY309) ($n = 96$) cells were analyzed for the percentage of binucleates with one or two GFP dots in one nucleus (types I and II, respectively) or one dot each in two nuclei (type III). (C) Wild-type (SGY263), *cin8*Δ (SGY5197), *kip1*Δ (SGY5347), and *kip3*Δ (SGY5190) cells arrested at prophase I by Ndt80 depletion and harboring homozygous CenV-GFP were analyzed by chromosome spreads for the number of GFP dots. One, two, or more than two 2 GFP dots were scored as paired, unpaired, or unpaired with noncohesed sister chromatids, respectively. (D) Cells analyzed in panel C were also observed for the Zip staining. $n = 150$ to 220 for panels C and D. (E) Strains in Fig. 1A were analyzed at the binucleated stage for the disjunction of CenV homologs ($n = 50$ to 110). Types I and II indicate disjunction and nondisjunction of the homologs, respectively. Error bars represent the standard deviations from the mean values obtained from three independent experiments, and "*n*" represents the number of cells scored. Bars, 2 μm.

*kip1*Δ mutant has been reported to be inviable (9, 16, 19, 47). Although the sporulation efficiencies of the *cin8*Δ, *kip3*Δ, and *cin8*Δ *kip3*Δ strains were similar (63%, 85%, and 70%, respectively) (Table 1) after 12 h of sporulation induction, strikingly, we observed a precipitous drop (approximately 16%) in the spore viability of the double mutant

TABLE 1 Sporulation efficiencies

Strain	% sporulation efficiency
Wild type	81
*cin8*Δ strain	62.9
*kip1*Δ strain	74.5
*kip3*Δ strain	85.2
*cin8*Δ *kip3*Δ strain	69.4

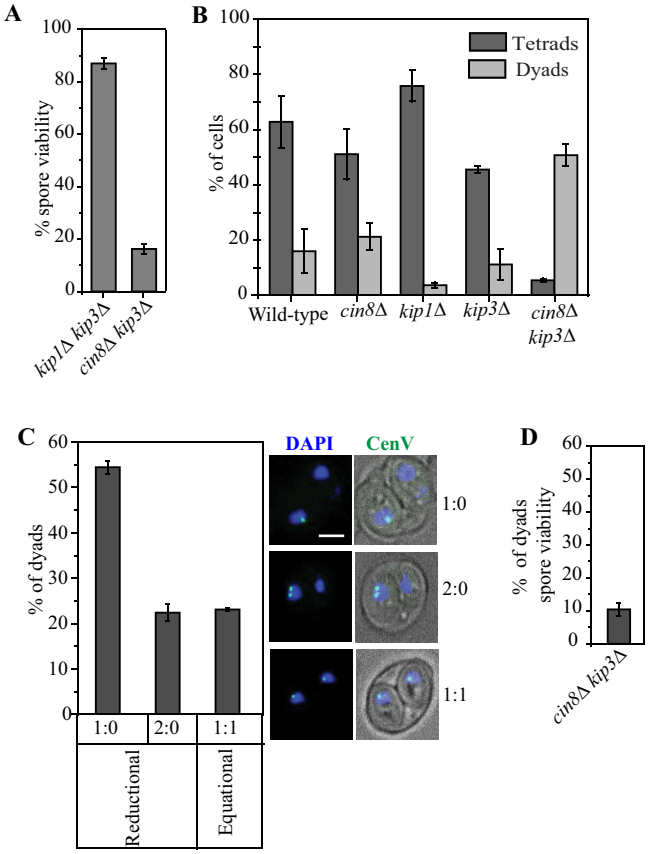

FIG 3 Meiosis in *cin8*Δ *kip3*Δ cells results in the frequent formation of dyads with aneuploid spores. (A and B) *kip1*Δ *kip3*Δ (SGY5104) ($n = 54$) and *cin8*Δ *kip3*Δ (SGY5089) ($n = 117$) cells were analyzed for spore viability (A) and the formation of dyads and tetrads (B) following 12 h of meiotic induction ($n = 195$ to 351). The maximum population of *cin8*Δ *kip3*Δ sporulated cells forms dyads, with a small population of tetrads. "*n*" represents the total numbers of tetrads dissected (A) and sporulated cells (B). (C) Percentages of dyads with one GFP dot each in two spores (1:1) and one or two GFP dots in one spore (1:0 or 2:0, respectively) in *cin8*Δ *kip3*Δ (SGY5154) cells ($n = 136$) harboring heterozygous CenV-GFP. Bar, 2 μm. (D) Spore viability of the dyads formed in *cin8*Δ *kip3*Δ (SGY5089) cells following meiosis at 30°C. Sixty dyads were dissected for viability estimation. Error bars represent the standard deviations from the mean values obtained from three independent experiments.

compared to the *cin8*Δ and *kip3*Δ single mutants (Fig. 1A and Fig. 3A). To further investigate the probable roles of Cin8 and Kip3 together in meiosis, we monitored meiotic progression in the wild type and the motor mutants and noticed that in comparison to the wild-type, *cin8*Δ, or *kip3*Δ strain, the *cin8*Δ *kip3*Δ double mutant proceeded through meiosis slowly, and the majority of the cells were arrested transiently at anaphase I, with one spindle and an improper disjunction of nuclei (Fig. 1Biii and Fig. 1C).

Given that Cin8 and Kip3 can cross-link and slide the antiparallel microtubules causing spindle elongation, our results indicate that cells lacking both Cin8 and Kip3 cause slow spindle elongation and defects in chromosome disjunction during meiosis I that might be responsible for the delay in spindle disassembly and completion of meiosis I. Due to this delay, around 50% of the *cin8*Δ *kip3*Δ cells proceeded to meiosis II without completing meiosis I, as assessed by the separation of sister chromatids on the meiosis I spindle and produced dyads (Fig. 3B and C). The inability to complete meiosis I due to a defect in spindle elongation but the ability to proceed to meiosis II and generate dyads with two diploid spores are hallmarks of the FEAR mutants (1, 2, 48, 49). Additionally, similar to the FEAR mutants (2), in *cin8*Δ *kip3*Δ cells, we also observed reductional segregation of chromosomes in the dyads, as both the heterozygously tagged CenV-GFP dots (sister chromatids) were found in one spore in 76% of the dyads

(Fig. 3C). However, cosegregation of the sister chromatids *per se* does not imply prevention of meiosis II in *cin8*Δ *kip3*Δ cells, since in many dyads, we observed stained nuclei that were not included in the spores, suggesting that massive missegregation had occurred during meiosis II as well. Consequently, the viability of the dyad spores obtained from *cin8*Δ *kip3*Δ cells was extremely poor (10%) (Fig. 3D).

We believe that the phenotypes of *cin8*Δ *kip3*Δ cells are similar to those of the FEAR mutants, as the Cdc14 phosphatase released by the FEAR network promotes spindle elongation through dephosphorylation of Cin8, which facilitates its binding to the spindles and sliding of the antiparallel microtubules (7, 31). However, the removal of Cin8 alone did not exhibit as severe a phenotype as that of the FEAR mutants due to functional redundancy in spindle elongation between Cin8 and Kip1/Kip3 and due to additional functions of the FEAR network (50). It is also expected that the FEAR mutant-like phenotypes observed in meiotic *cin8*Δ *kip3*Δ cells will also be observed in mitosis. Since the FEAR mutants exhibit a delay in mitotic exit (51), the wild type and the motor mutants were released synchronously using α-factor into fresh yeast extract-peptone-dextrose (YPD) medium to compare the paces of mitosis. As observed for the *esp1-1* FEAR mutant (51, 52), we observed a delay in cell cycle progression in *cin8*Δ and *cin8*Δ *kip3*Δ cells. Wild-type, *kip1*Δ, and *kip3*Δ cells completed one cycle of mitosis in approximately 55 min, while in the *cin8*Δ and *cin8*Δ *kip3*Δ mutants, it was delayed (around 75 min) (as shown by the dashed and dotted lines, respectively, in Fig. S1A at http://www.bio.iitb.ac.in/~santanu/wp-content/uploads/2020/05/Supplementary_file-final.pdf). In the time window between 90 and 100 min (see Fig. S1B at the URL mentioned above), the wild-type, *kip1*Δ, and *kip3*Δ strains exhibit a second peak for metaphase cells, while the *cin8*Δ strain demonstrates only one peak, whereas in the *cin8*Δ *kip3*Δ strain, the same peak is broadened and further extended until 105 min, suggesting that the metaphase-to-anaphase transition is maximally delayed in the double mutant. Additionally, we also observed a phenotype in the *cin8*Δ and *cin8*Δ *kip3*Δ mutants at equal frequencies, where we found a persistent population of cells with elongated nuclei spanning the mother cell and daughter bud but with a bipolar spindle of a metaphase-specific length (type II) (see Fig. S1C at the URL mentioned above). Such a phenotype could be due to an inability to extend the spindle but with the to-and-fro movement of the short spindle resulting in nuclear elongation, which has been observed previously with metaphase-arrested short spindles (53).

From the above-described results, it is apparent that the absence of both Cin8 and Kip3 causes defects in spindle elongation and the metaphase-to-anaphase transition in both mitosis and meiosis. However, it is apparent that while in meiosis, *cin8*Δ *kip3*Δ cells show more defects in spindle elongation and in the metaphase-to-anaphase transition than the single mutants, such a difference is absent in mitosis. Consequently, in contrast to the poor spore viability following meiosis observed for the *cin8*Δ *kip3*Δ mutant (Fig. 3A), we failed to observe any difference in viabilities among the wild type, the single mutants, and the *cin8*Δ *kip3*Δ double mutant following mitosis (see Fig. S1D at the URL mentioned above). This is further supported by the fact that while the pace of meiosis was affected to a greater extent in the *cin8*Δ *kip3*Δ mutant than in the wild type or the single mutants (Fig. 1B), the mitotic growth rates were not affected to that extent (see Fig. S1E at the URL mentioned above). These results suggest that the loss of both Cin8 and Kip3 perhaps causes some meiosis-specific defects, as revealed below.

Meiotic chromosome segregation is largely perturbed in the *cin8*Δ *kip3*Δ mutant. To examine if there are any meiosis-specific defects in the *cin8*Δ *kip3*Δ mutant, we sought to investigate meiotic chromosome segregation under these conditions. We used wild-type, *cin8*Δ *kip3*Δ and *kip1*Δ *kip3*Δ double mutant, and the corresponding single mutant cells where both homologs of chromosome V were marked with GFP. Since we observed that the *cin8*Δ *kip3*Δ mutant did not sporulate at a temperature of 33°C, meiosis induction was carried out at 30°C. We analyzed tetranucleated cells to ensure that both meiosis I and meiosis II had occurred. Wild-type, *kip3*Δ, *kip1*Δ, and *kip1*Δ *kip3*Δ cells mostly showed (100%, 92%, 84%, and 88%, respectively) four nuclei

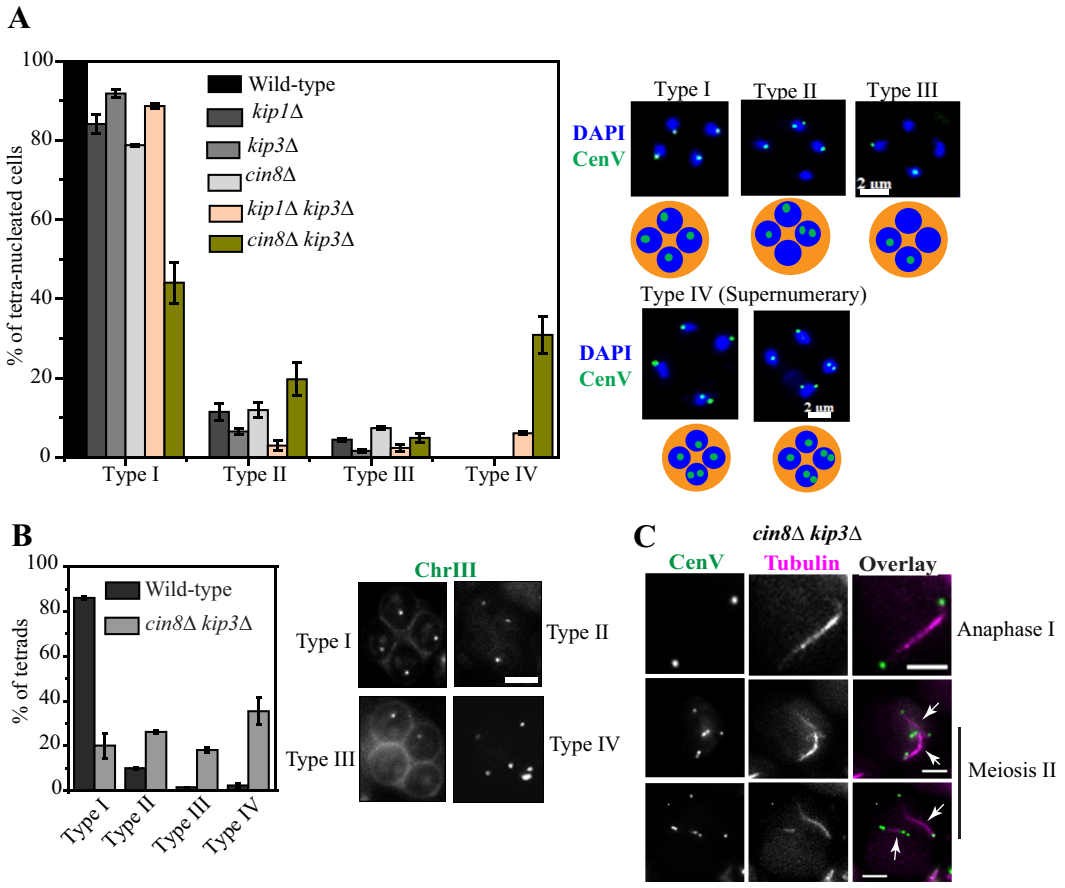

FIG 4 The *cin8*Δ *kip3*Δ mutant generates aneuploid tetranucleated cells showing supernumerary GFP foci of the marked chromosomes. (A) Tetranucleated cells of the wild-type (SGY5001), *cin8*Δ (SGY315), *kip1*Δ (SGY317), *kip3*Δ (SGY314), *kip1*Δ *kip3*Δ (SGY5104), and *cin8*Δ *kip3*Δ (SGY5089) strains harboring homozygous CenV-GFP were analyzed for meiotic chromosome segregation at 30°C ($n = 100$ to 309). "*n*" represents the number of tetranucleated cells scored for chromosome segregation. (B) Tetrads from the wild-type (SGY5407) ($n = 129$) and *cin8*Δ *kip3*Δ (SGY5329) ($n = 119$) strains harboring homozygous ChrIII-GFP marked at the *LEU2* locus 22 kb away from the centromere were analyzed as described above for panel A. Type I represents one GFP focus in each of the four spores, whereas types II and II represent four GFP foci in three or two spores, respectively. Type IV is the tetrad with >4 GFP foci. (C) Supernumerary CenV-GFP foci are observed only in those *cin8*Δ *kip3*Δ cells (SGY5385) that are in meiosis II, as judged by the presence of two spindles (marked by arrows). Error bars represent the standard deviations from the mean values obtained from three independent experiments. Bars, 2 μm.

with one GFP dot in each nucleus (type I) (Fig. 4A), which was reduced slightly in *cin8*Δ cells and largely in *cin8*Δ *kip3*Δ cells (79% and 44%, respectively). The type II and III categories, having GFP dots in three or two nuclei, respectively, and which account for missegregation of the chromosomes, were found correspondingly more often in the mutants. Unexpectedly, a significant population of tetranucleates (approximately 30%) harboring >4 (termed "supernumerary") CenV-GFP dots was found in *cin8*Δ *kip3*Δ cells (type IV category) (Fig. 4A), while a minute population of this category was observed in *kip1*Δ *kip3*Δ cells (6%). The difference observed between the double mutants can be expected since Cin8 is known to have more significant cell cycle functions than Kip1 from a previous mitotic study (16). The supernumerary GFP dot phenotype is not specific for chromosome V since the same phenotype was also observed (approximately 35%) (type IV) in the *cin8*Δ *kip3*Δ mutant when chromosome III (ChrIII) was marked using the LacO/LacI-GFP system at the pericentromeric region (22 kb away from CenIII) (Fig. 4B). To determine the stage of the cell cycle at which these supernumerary foci start appearing, Tub1 was N terminally tagged with cyan fluorescent protein (CFP) in the *cin8*Δ *kip3*Δ strain harboring homozygous CenV-GFP. Chromosome abnormality was found only in the cells with two spindles, suggesting that >4 foci were generated in cells that had passed through meiosis II (Fig. 4C). This numerical abnor-

mality is specific for meiosis and did not occur due to aneuploidy generated as a legacy of an error during previous mitosis since we failed to obtain >2 GFP dots before entry into meiosis (see Fig. S2A at http://www.bio.iitb.ac.in/~santanu/wp-content/uploads/2020/05/Supplementary_file-final.pdf) or during any stage of mitosis (see Fig. S2B at the URL mentioned above) in *cin8*Δ *kip3*Δ cells.

Chromosome breakage occurs in *cin8*Δ *kip3*Δ cells during meiosis II. We next sought to address the reason for the generation of supernumerary GFP foci in *cin8*Δ *kip3*Δ cells. At least two possibilities can be envisaged for this. First, leaky chromosome replication between meioses I and II may amplify the operator arrays and cause >4 GFP foci. However, this possibility seems unlikely because if there is leaky replication of the operator array, due to close proximity (within 1.4 kb), CenV would also have been replicated, and in that case, >4 kinetochore foci would have been observed. However, we found the normal four Ndc10 (kinetochore) foci in 100% of cells with supernumerary CenV foci (see Fig. S2C at the URL mentioned above). Second, due to an imbalance of spindle force acting on the centromeres, the chromosomes may break, and since the operator arrays in our assays remain closed to the centromere, the arrays can also break to give >4 GFP foci. Given the functions of the motors in moderating spindle-chromosome interactions through force generation, the latter possibility is more likely. To investigate if there is indeed any chromosome breakage, a single-cell gel electrophoresis assay, known as the comet assay, was performed (54). As it is difficult to lyse the tetrad because of the robust spore wall, cells were analyzed for chromosome breakage at the tetranucleated stage before the formation of the spore wall. For the comet assay, the cells were released synchronously in meiosis. At the time of harvesting of the cells, there were >50% tetranucleated cells (observed by nucleus staining) in all the strains utilized for the assay, and ≥17% of the cells were at the binucleated stage (Fig. 5A). This observation suggests the completion of S phase in most of the cells and negates the possibility of the presence of any replication intermediates that might give a tail-like appearance in the comet assay. H_2O_2 (10 mM)-treated cells were used as a positive control for breakage (55). Interestingly, we obtained a notable population of DNA masses that formed tails or a comet phenotype in *cin8*Δ *kip3*Δ (approximately 20%) cells compared to wild-type (2.5%) or *cin8*Δ (1%) cells, while in the H_2O_2-treated sample, almost 46% of the cells exhibited the comet phenotype (Fig. 5B). To quantify the defect, we compared the percentages of DNA in the head and tail parts of the comet among the test samples (see Materials and Methods) (56). A reduction in the percentage of DNA in the head region is accompanied by an increase in the percentage of DNA in the tails of H_2O_2-treated and *cin8*Δ *kip3*Δ spheroplasts (Fig. 5C). The lack of tail structures in wild-type and *cin8*Δ cells is not due to the presence of sporulated cells that are resistant to Zymolyase treatment, since in the population of tetranucleated cells used for the comet assay, approximately 89%, 59%, and 66% of wild-type, *cin8*Δ, and *cin8*Δ *kip3*Δ cells were nonsporulated, respectively (Fig. 5D). Furthermore, the spores contained the spore wall, which was not visible in the spheroplasted nuclei of the above-described test samples under a bright-field microscope (Fig. 5E). Note that for comparison among the test samples, only spheroplasted cells were analyzed for the detection of the comets. Based on these criteria, the above-described results suggest that chromosome breakage occurs in *cin8*Δ *kip3*Δ cells.

To further reconfirm the chromosome breakage, we looked at the localization pattern of Rad52, which is required for the repair of DNA double-stranded breaks (DSBs) generated due to intrinsic or extrinsic factors (57–60). In meiosis, at prophase I, programmed DSBs occur for recombination, and consequently, Rad52 foci are visible at this stage in the wild type. However, once the DSBs are repaired, the average number of Rad52 foci reduces but persists in later stages of meiosis (61, 62). We counted and compared the Rad52-enhanced GFP (EGFP) foci in wild-type, *cin8*Δ, and *cin8*Δ *kip3*Δ chromosome spreads harboring 1 SPB within a single nucleus (prophase I stage) (Fig. 5F); 2 SPBs, 1 in each of the 2 nuclei (anaphase I stage) (Fig. 5G); and 4 SPBs, 1 in each of the 4 nuclei (anaphase II/post-meiosis II stage) (Fig. 5H). At prophase I, we observed

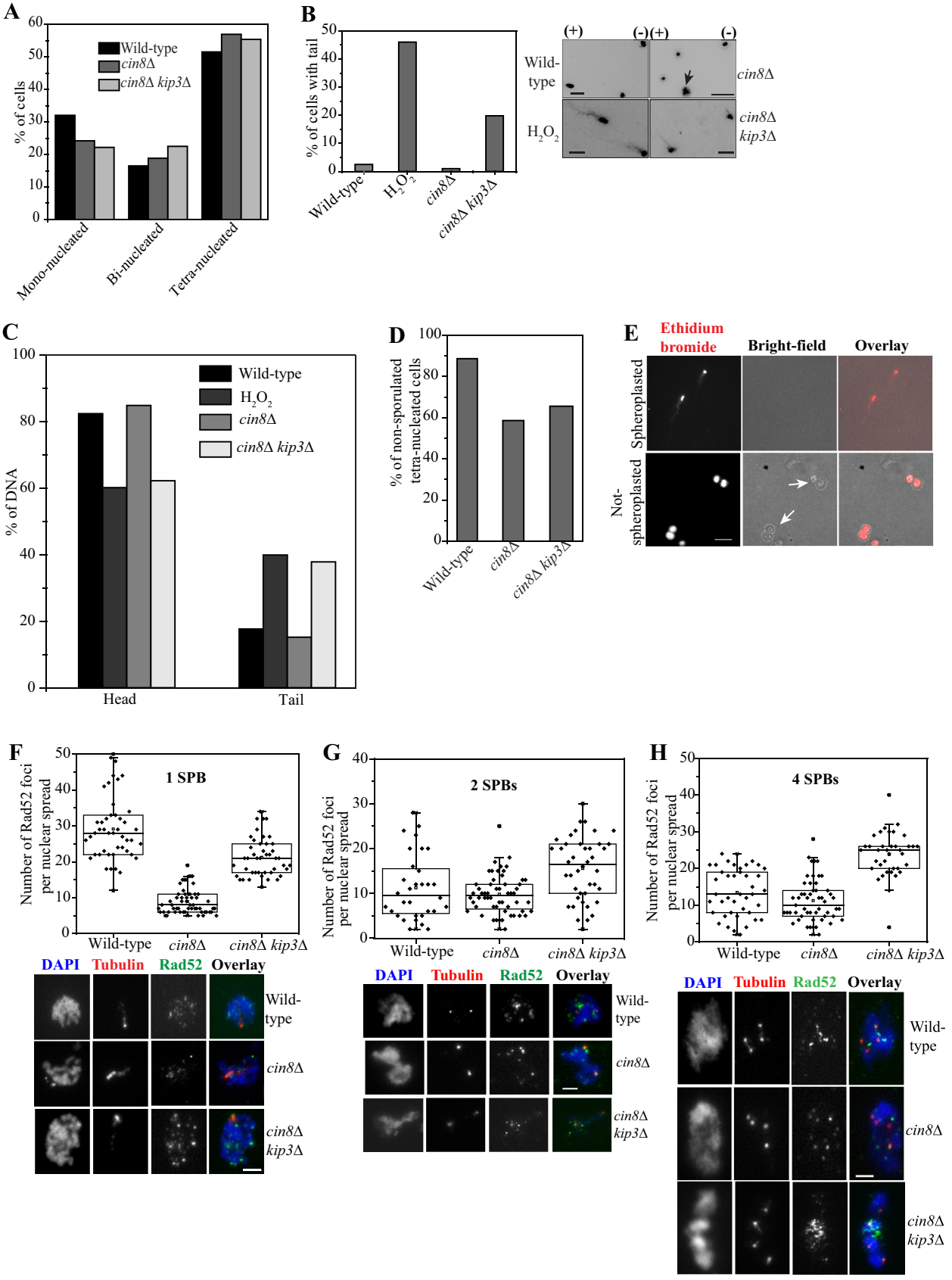

FIG 5 *cin8Δ kip3Δ* cells cause DNA breakage as they proceed through meiosis. (A) Nuclear stages of meiotic cells harvested for the comet assay (see Materials and Methods) from the sporulation medium (SPM) culture before the formation of the tetrads, which is at 8 h for *cin8Δ kip3Δ* (SGY5089)

(Continued on next page)

an average of 29 foci in wild-type spreads, which was reduced to 9 ± 3 foci in *cin8*Δ spreads (Fig. 5F), which is consistent with the defective homolog pairing observed in *cin8*Δ cells (Fig. 2C). However, in *cin8*Δ *kip3*Δ cells, the average count was nearly 21, which suggests that the loss of Kip3 by an unknown mechanism rescues the defect of the *cin8*Δ mutant. While analyzing the spreads at anaphase I, we noticed no significant difference in Rad52-EGFP staining between wild-type and *cin8*Δ cells (wild-type spreads, 11 ± 7 foci; *cin8*Δ spreads, 10 ± 4 foci) (Fig. 5G) but observed a slight increase in staining for the double mutant (*cin8*Δ *kip3*Δ spreads, 15 ± 7 foci) (Fig. 5G). However, a drastic accretion in Rad52-EGFP staining was observed in *cin8*Δ *kip3*Δ spreads at anaphase II/post-meiosis II (tetranucleated stage) over the wild-type or *cin8*Δ spreads (wild-type spreads, 13 ± 6 foci; *cin8*Δ spreads, 11 ± 6 foci; *cin8*Δ *kip3*Δ spreads, 24 ± 6 foci) (Fig. 5H). These results indicate that as *cin8*Δ *kip3*Δ cells pass through meiosis II, they accumulate DNA damage in the form of DSBs (Fig. 4C).

Previously, we noticed supernumerary SPB formation in kinetochore mutants as the cells entered meiosis II (63). As both Cin8 and Kip3 also have some functional roles at the centromeres, we reasoned that in *cin8*Δ *kip3*Δ cells, following interphase II (stage between meioses I and II), maybe >4 SPBs or spindle poles are generated, and the resulting extra pole(s) may cause an imbalance of force and, hence, chromosome breakage. However, analysis of tetranucleated *cin8*Δ *kip3*Δ cells harboring >4 CenV-GFP foci showed only 4 SPBs (see Fig. S3 at http://www.bio.iitb.ac.in/~santanu/wp-content/uploads/2020/05/Supplementary_file-final.pdf), indicating that multipolarity is not the cause of chromosome breakage.

The *cin8*Δ *kip3*Δ strain hinders cohesin removal from chromatin in meiosis. In budding yeast, cohesin is removed from the chromosome arms during anaphase I, while the removal of centromeric cohesin occurs during meiosis II. However, in FEAR mutants, the loss of cohesin from the arms is delayed during anaphase I (2). Since we noticed that *cin8*Δ *kip3*Δ cells exhibit phenotypes similar to those of FEAR mutants during meiosis (Fig. 1Biii and Fig. 3B), we therefore investigated if the double mutant is compromised in cohesin removal. We monitored Rec8-EGFP staining at different stages of meiosis in wild-type and *cin8*Δ *kip3*Δ cells. Meiotic stages were determined on the basis of the number of and distance between the Spc42 foci. Centromeric Rec8 was judged by its staining to be present only in the vicinity of the SPBs due to the proximity of the centromeres to the SPBs, whereas nuclear Rec8 comprised of arm plus centromeric Rec8, was identified by its presence spanning a broader region between the two SPBs (Fig. 6A and B). We observed that for the wild type, 64% of anaphase I cells displayed centromeric Rec8, which was reduced to 35% in *cin8*Δ *kip3*Δ cells (Fig. 6C). Rather, we noticed more cells with nuclear Rec8 in the double mutant (65%) than in the wild type (36%), suggesting a defect in cohesin removal during the metaphase I-to-anaphase I transition. Given that cohesin removal is completed during meiosis II, strikingly, nuclear Rec8 was observed even during the meiosis II stage in a staggering population (45%) of *cin8*Δ *kip3*Δ cells, whereas for the wild type, this population was insignificant (3%) (Fig. 6A, B, and D). It is possible that the expression of Rec8 is upregulated in *cin8*Δ *kip3*Δ cells, causing its accumulation and, hence, a defect in its efficient removal. To test this, we compared the levels of Rec8 expression between the

FIG 5 Legend (Continued)
cells, 7 h for *cin8*Δ (SGY315) cells, and 5 h for wild-type (SGY40) cells. (B) Cells analyzed as described above for panel A were used for the comet assay. As a positive control, wild-type cells were treated with 10 mM H_2O_2 for 30 min at 4°C. The histograms correspond to the percentages of the cells that formed comets. Representative gel images (with "+" and "−" polarities) show ethidium bromide-stained DNA from each strain. "+" and "−" indicate the anode and the cathode, respectively. The arrow indicates an unspheroplasted cell. A total of 80 to 156 nuclei were observed for comet formation. Bars, 5 μm. (C) Percentages of DNA in the tail and head regions were calculated as described in Materials and Methods and plotted. (D) Cells with four nuclei observed in panel A were analyzed for the presence or absence of spore wall formation. (E) Representative images showing that, compared to spheroplasted cells, the cell wall is visible in cells that are not spheroplasted. Arrows indicate sporulated cells. (F to H) Chromosome spreads showing Rad52-EGFP foci stained using anti-GFP antibody in the wild-type (SGY5414), *cin8*Δ (SGY5422), and *cin8*Δ *kip3*Δ (SGY5415) strains. At least 40 spreads were analyzed for each type. Spindle poles marked by anti-α-tubulin antibody were used to judge the cell cycle stage of the spreads. Foci were counted after merging of the z-stacks, with the maximum intensities for tubulin and Rad52 keeping the threshold the same for all the fields. One tubulin dot (1 SPB) within one DAPI mass represents prophase I, while 2 dots (2 SPBs, 1 dot each in two DAPI masses) represent anaphase I, and 4 dots (4 SPBs, 1 dot each in four DAPI masses) represent the meiosis II stage. Bars, 2 μm.

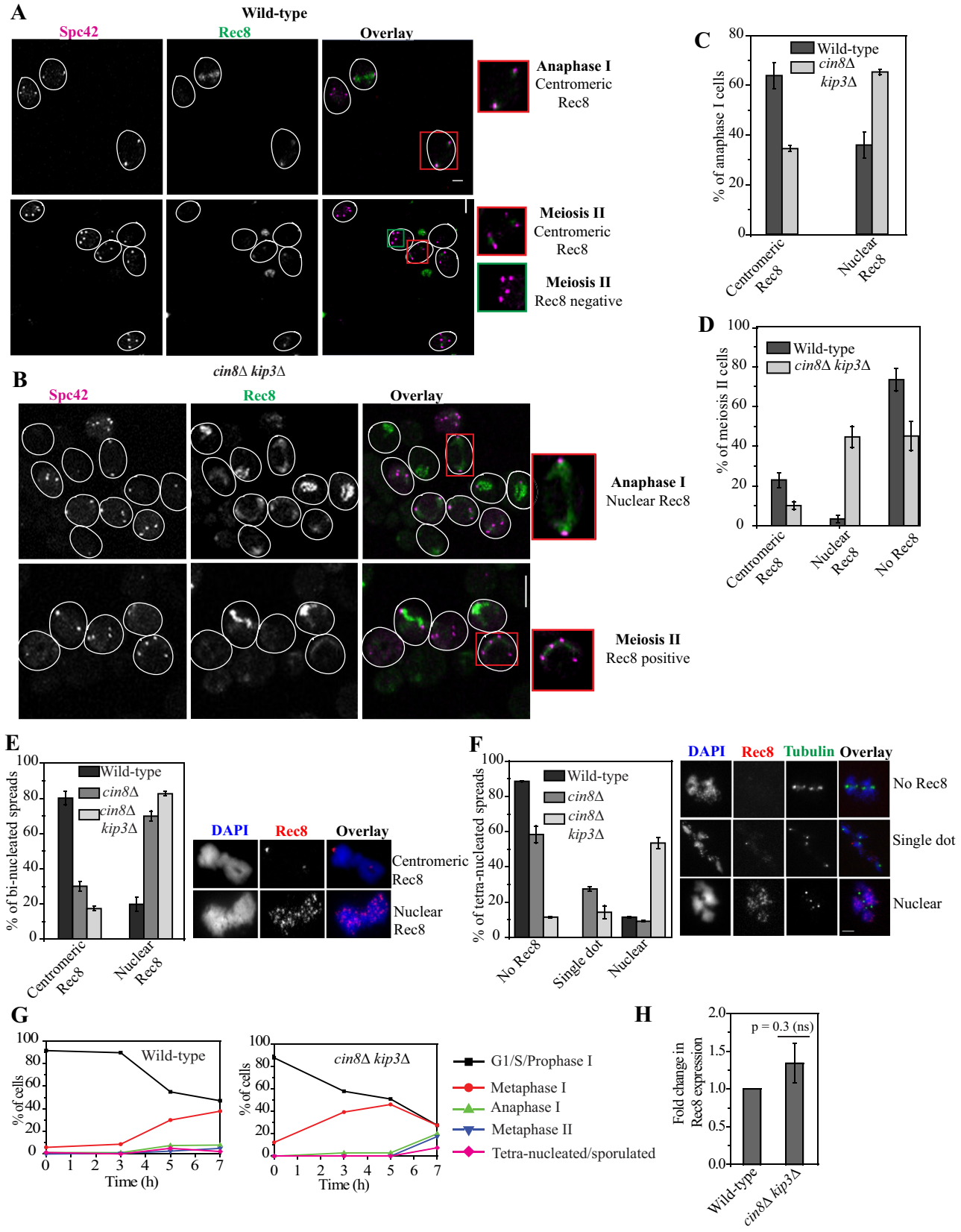

FIG 6 Removal of Rec8 cohesin is defective in the *cin8Δ kip3Δ* mutant. (A to D) Wild-type (SGY5557) and *cin8Δ kip3Δ* (SGY5523) cells harboring Rec8-EGFP and Spc42-CFP were analyzed for Rec8 localization at different stages of meiosis. (A) Representative images where Rec8 staining appearing as two tight-knit dots at the vicinity of each of the two SPBs or as a single such dot each between the two SPBs of two pairs was scored as centromeric Rec8

(Continued on next page)

wild-type and *cin8*Δ *kip3*Δ strains at the mRNA level. Since Rec8 expression peaks during the early stage of meiosis (64), we examined RNA levels at this stage. Based on the meiotic progression assay, we observed that following meiosis induction, at the 5-h time point, both strains harbored similar populations of metaphase I cells (Fig. 6G), and hence, RNA was isolated at this time point and quantified by reverse transcription followed by quantitative PCR-quantitative PCR (RT-qPCR). However, we failed to detect any significant difference in Rec8 levels between the wild type and the double mutant (Fig. 6H). This suggests that the greater Rec8 staining observed for the *cin8*Δ *kip3*Δ strain during anaphase I and subsequent stages is not due to an increase in its expression but is due to a defect in its removal.

We obtained similar results in chromosome spreads immunostained for Rec8-EGFP, where both binucleated and tetranucleated spreads had high levels of nuclear Rec8 (82% and 54%, respectively) in the *cin8*Δ *kip3*Δ strain with respect to the wild type (19% and 11%, respectively) (Fig. 6E and F). Notably, we observed that in *cin8*Δ cells, nuclear Rec8 also persisted in a larger population of binucleated spreads (70%) (Fig. 6E). However, in the majority of the spreads at the tetranucleated stage, Rec8 appeared as a single dot, indicating the presence of a negligible amount on the chromatin, in contrast to the dispersed Rec8 signal present all over the chromatin in the double mutant in a higher percentage of the spreads (Fig. 6F). Altogether, these results suggest that a prolonged cohesin-chromatin association occurs in *cin8*Δ *kip3*Δ cells and, to a lesser extent, in *cin8*Δ cells. Due to this defect and the associated delay in spindle elongation and disassembly, *cin8*Δ and *cin8*Δ *kip3*Δ cells show a delay in the meiosis I-to-meiosis II transition (Fig. 1Biii). It is tempting to speculate that due to a higher level of cohesion retention in *cin8*Δ *kip3*Δ cells, the chromosomes cannot disjoin properly when subjected to pulling force exerted by the other motors during anaphase I and anaphase II spindle elongations, and they eventually break, causing very low spore viability.

As we observed a delay in spindle elongation and cell cycle progression in *cin8*Δ and *cin8*Δ *kip3*Δ cells, it is critical to address if the prolonged retention of Rec8 on chromatin is due to a delay in the degradation of securin (Pds1), a condition that releases separase to cleave Rec8. Under unperturbed conditions, Pds1 is degraded during the metaphase I-to-anaphase I transition following a reappearance in metaphase II and degradation in anaphase II. We monitored the levels of Rec8 and Pds1 through synchronized meiosis in wild-type, *cin8*Δ, and *cin8*Δ *kip3*Δ cells by immunoblotting (Fig. 7A and B). As described above (Fig. 1B), the pace of meiosis was delayed in *cin8*Δ *kip3*Δ cells compared to wild-type and *cin8*Δ cells (Fig. 7C); Pds1 degradation in the same strains also followed the same regime (Fig. 7A and B). Notably, with the disappearance of Pds1, all Rec8 was removed in wild-type cells, while removal was deferred in *cin8*Δ cells and, to a greater extent, in *cin8*Δ *kip3*Δ cells (Fig. 7A and B). Consistent with our cell biological data (Fig. 6), we noticed that in the double mutant, a significant level of Rec8 was persistent even at 15 h in meiosis, when around 90% of the cells had either entered into anaphase II or sporulated, whereas in such cells of either the wild-type or the *cin8*Δ

FIG 6 Legend (Continued)
at anaphase I or meiosis II (metaphase II and anaphase II), respectively. Meiosis II cells with no Rec8 staining were also scored. (B) Representative images where Rec8 staining appearing in a broader region close to the SPBs or between the SPBs was scored as nuclear Rec8 (arm plus centromeric) at anaphase I or at meiosis II, respectively. (C and D) Percentages of anaphase I (C) and meiosis II (D) cells with the types of Rec8 staining in wild-type and *cin8*Δ *kip3*Δ strains. For panels C and D, 148 and 267 cells were analyzed for the wild-type and *cin8*Δ *kip3*Δ strains, respectively. Bars, 5 μm. (E and F) Chromosome spreads from wild-type (SGY5497) ($n = 83$), *cin8*Δ (SGY5501) ($n = 114$), and *cin8*Δ *kip3*Δ (SGY5500) ($n = 183$) cells harboring Rec8-EGFP were monitored at different stages of meiosis by EGFP immunostaining. (E) Quantitative analysis of Rec8 localization as only two foci (centromeric Rec8) or distributed throughout the chromatin (nuclear Rec8) in binucleated chromosome spreads. Representative images of each type are shown on the right. (F) Quantitative analysis of Rec8 localization with a tiny (single dot) or large (nuclear) appearance on the chromosome spreads from the tetranucleates. The tetranucleated stage of the spreads was determined by tubulin immunostaining. *cin8*Δ *kip3*Δ cells show significant Rec8 throughout the chromatin (nuclear), even in the tetranucleated stage. Representative images of each type are shown on the right. (G) Wild-type (SGY5533) and *cin8*Δ *kip3*Δ (SGY5534) strains tagged with Rec8-6HA were analyzed for different stages of meiosis at the indicated time points by tubulin immunostaining and DAPI staining. (H) Normalized mRNA expression level of Rec8 in the strains used for panel G. The Rec8 mRNA expression level does not change between the wild-type and *cin8*Δ *kip3*Δ strains. The values from the three independent biological replicates were averaged and plotted. Error bars represent the standard deviations from the mean values. A P value of ≥ 0.05 is considered nonsignificant (ns). Bars, 2 μm.

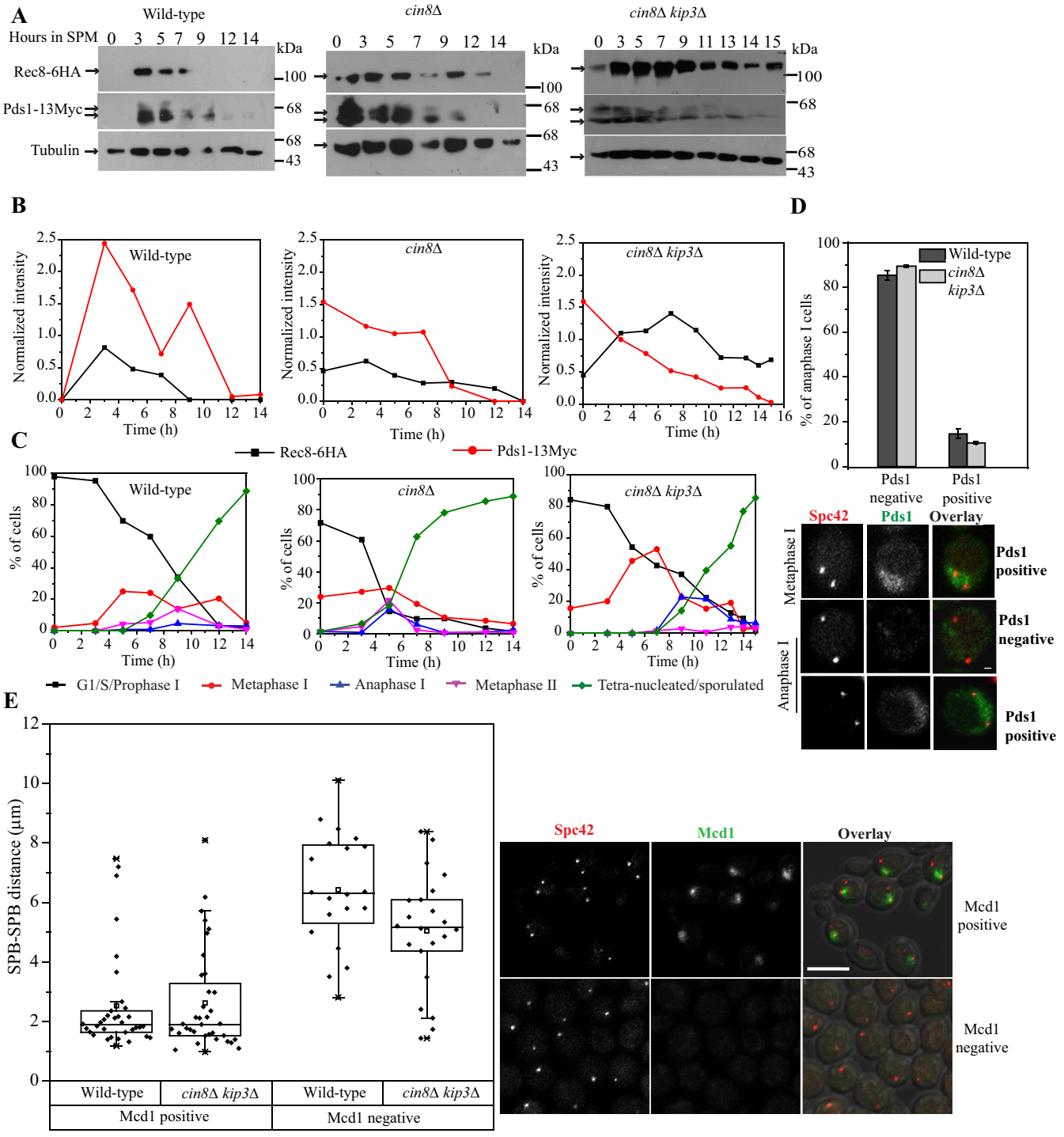

FIG 7 The *cin8*Δ *kip3*Δ mutant perturbs the coordination between Pds1 and Rec8 degradation in meiosis but does not affect the dynamics of Mcd1 removal in mitosis. (A) Western blot analysis of wild-type (SGY5534), *cin8*Δ (SGY5532), and *cin8*Δ *kip3*Δ (SGY5533) cells for the levels of Rec8-6HA and Pds1-13Myc at the indicated time points during meiotic progression. Tubulin was used as a loading control. (B) Densitometric analysis of Rec8-6HA and Pds1-13Myc signals obtained in panel A after normalization to the tubulin signal using ImageJ software. As evident from the graph, the drop in the Rec8 level, unlike Pds1, is much slower in *cin8*Δ *kip3*Δ than in wild-type or *cin8*Δ cells. (C) Percentages of prophase I, metaphase I, anaphase I, metaphase II, and anaphase II/sporulated cells determined by tubulin immunostaining at the time points utilized for Rec8-6HA and Pds1-13Myc detection in panels A and B ($n \geq 90$ cells for each time point). (D) Analysis of Pds1-EGFP localization in wild-type (SGY5570) ($n = 44$) and *cin8*Δ *kip3*Δ (SGY5567) ($n = 75$) cells during the anaphase I stage determined by the distance between the two SPBs marked with Spc42-mCherry as shown in the representative images at the bottom. Pds1 staining under wild-type conditions, i.e., at the metaphase I stage, is also represented. (E) Localization of Mcd1-EGFP in wild-type (SGY5629) and *cin8*Δ *kip3*Δ (SGY5630) cells corresponding to the three-dimensional (3D) distances between the two spindle poles marked by Spc42-mCherry. Fields of view of metaphase ($\leq$1.2-μm distance) and anaphase ($\geq$2.5-μm distance) cells show the presence and absence of Mcd1-EGFP, respectively. Error bars represent the standard deviations from the mean values obtained from three independent experiments. Bar, 2 μm.

strain, Rec8 was absent (Fig. 7A to C). Live-cell imaging of Pds1-EGFP also revealed that there is no difference in Pds1 stability on the anaphase I spindle between the wild type and the double mutant (Fig. 7D). These results suggest that protracted Rec8 retention on chromatin in *cin8*Δ *kip3*Δ cells is not due to a biochemical delay imposed by persistent Pds1.

The failure of proper cohesin removal in post-anaphase I *cin8*Δ *kip3*Δ cells instigated us to examine if a similar defect prevails in mitosis. For the estimation of Mcd1 (mitotic cohesin) localization with respect to the distinct mitotic stages, cells were released synchronously from G_1 arrest and examined for the presence or absence of an Mcd1-GFP nuclear signal. With reference to the distances between the SPBs, we found no significant difference in Mcd1-EGFP staining between wild-type and *cin8*Δ *kip3*Δ cells. The cells with interpolar distances in the range of 1.2 to 2.2 μm (metaphase/preanaphase) were positive for Mcd1-GFP, while beyond that (postanaphase), no Mcd1 staining was visible (Fig. 7E). These results indicate that mitotic cohesin removal is not perturbed in *cin8*Δ *kip3*Δ cells.

The *cin8*Δ *kip3*Δ strain causes homolog nondisjunction and aberrant meiosis II. As the defect in cohesin removal hinders homolog separation during meiosis I (65, 66), we analyzed homolog segregation in wild-type and *cin8*Δ *kip3*Δ binucleated cells harboring homozygous CenV-GFP (Fig. 8A). Such cells with proper homolog disjunction will exhibit an equal number of CenV-GFP foci in each nucleus (2:2; type I), whereas nondisjunction will result in an unequal distribution of GFP foci (1:0, 1:3, and 4:0; type II). We detected the type II phenotype in approximately 26% of *cin8*Δ *kip3*Δ cells, compared to 12% of wild-type cells. Notably, a unique third category (around 17%) (type III) was observed only in *cin8*Δ *kip3*Δ cells, where CenV-GFP dots were present in the middle of a stretched DAPI (4′,6-diamidino-2-phenylindole) signal, where due to incomplete segregation, instead of two equal masses, DAPI is stained as one single elongated mass. We believe that the type III phenotype was generated as the sustained cohesin perturbs chiasma resolution and impedes the disjunction of the homolog, since we observed a significant reduction in the distance between the two homologs in binucleated meiosis I cells (Fig. 8B). In support of this, the removal of chiasmata by the *spo11*Δ strain resulted in a reduction of the type III phenotype of *cin8*Δ *kip3*Δ *spo11*Δ cells (Fig. 8A). However, the *spo11*Δ strain caused an increased type II frequency, as the loss of homolog pairing is known to perturb homolog biorientation and disjunction (65, 67).

A blockage in Rec8 cleavage in the *esp1-1* separase mutant hinders nuclear separation; however, following prolonged arrest, the cells embark on abrupt meiosis II (65). Since homolog nondisjunction was found to be impaired in *cin8*Δ *kip3*Δ binucleated cells, which include both anaphase I as well as metaphase II cells (Fig. 8A), we examined meiosis I and II nuclear segregations in cells harboring two SPBs (Fig. 8C) and four SPBs (Fig. 8D), respectively. Given that cohesin retention in the *cin8*Δ *kip3*Δ strain is not due to Pds1 stability, i.e., cell cycle arrest (Fig. 7A to D), we argued that these cells would progress through meiosis I in spite of having a physical barrier in nuclear separation. As expected, we observed a significant population of anaphase I cells of the *cin8*Δ *kip3*Δ strain with incomplete nuclear division, as evident from the "stretched" nuclear morphology (approximately 40%) (Fig. 8C).

We also observed a meager population (approximately 10%) of anaphase I cells with three connecting nuclear lobes ("crossed" morphology) only for the *cin8*Δ *kip3*Δ strain. This category of DAPI segregation resembles the one obtained for FEAR mutants resulting from the initiation of meiosis II on the meiosis I spindle (2). The population of cells in the stretched and crossed categories either evade meiosis II, forming dyads (Fig. 3B), or abruptly enter meiosis II, where they showed mostly asymmetric (26%) and no nuclear (mononucleates) (41%) separation with 4 SPBs (Fig. 8D). Similar phenotypes were observed in *mam1*Δ cells due to delayed nuclear division (68). Furthermore, due to the prolonged anaphase I and the subsequent abrupt initiation of meiosis II, there was a significant difference in the lengths of the two spindles in meiosis II in around 34% of *cin8*Δ *kip3*Δ cells (Fig. 8E). This phenotype is similar to the ones observed in

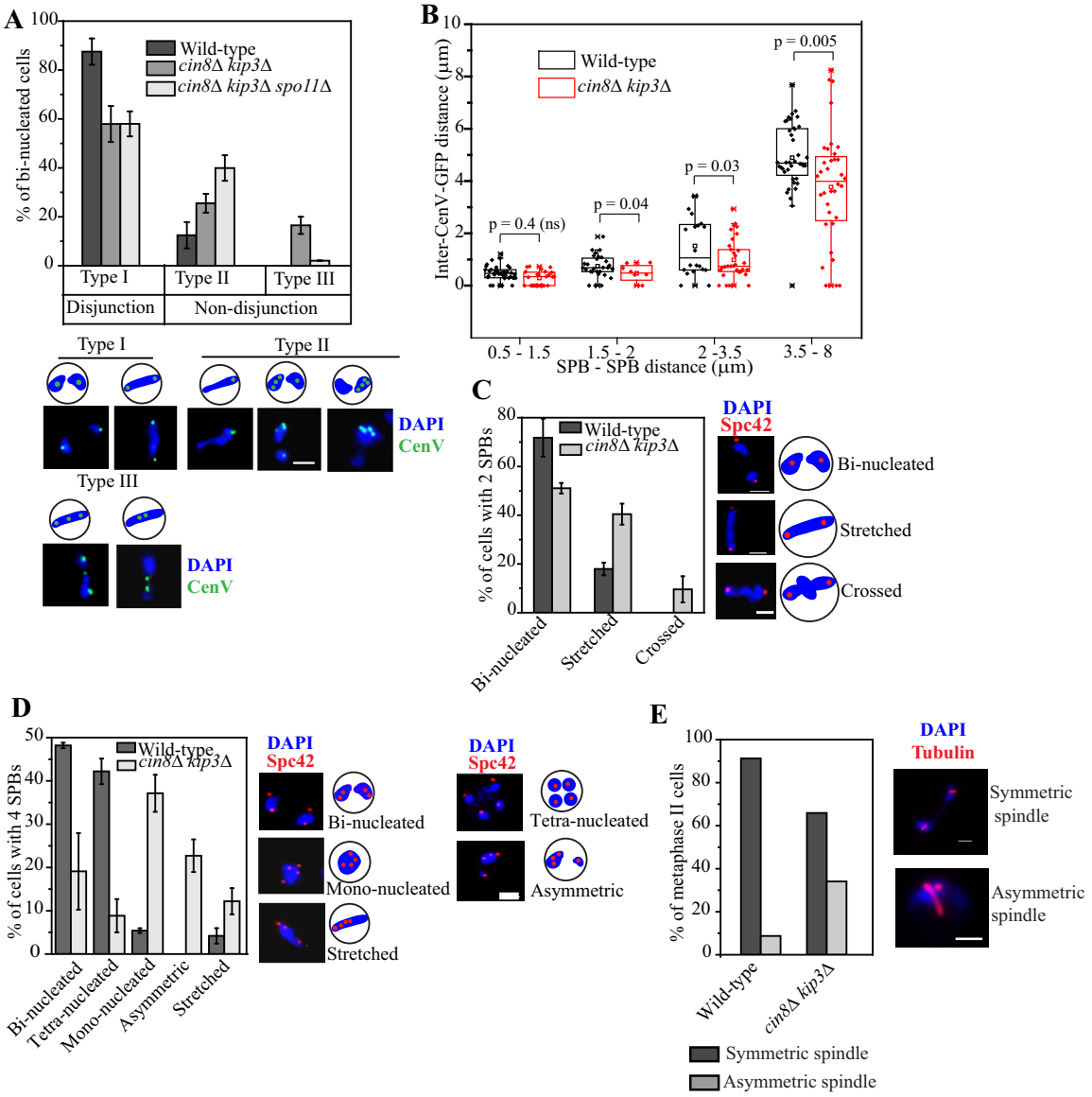

FIG 8 Homologous chromosomes and nuclear separation are impeded in *cin8*Δ *kip3*Δ cells. Wild-type (SGY9002) and *cin8*Δ *kip3*Δ (SGY5338) cells harboring homozygously marked CenV-GFP and Spc42-mCherry were released into meiosis at 30°C and analyzed for the homolog (CenV) and nuclear segregation. (A) Segregation of the CenV-GFP homologs at the binucleated stage for wild-type ($n = 185$), *cin8*Δ *kip3*Δ ($n = 167$), and *cin8*Δ *kip3*Δ *spo11*Δ (SGY5444) ($n = 97$) cells. Representative images for the types of CenV homolog separation are shown. (B) 3D distances between the two CenV-GFP homologs plotted with respect to the interpolar (SPB-SPB) distances. The distances were measured using Imaris software (see Materials and Methods). (C and D) Nuclear separation in meiotic cells harboring 2 SPBs (C) and 4 SPBs (D) (for panel C, $n = 70$ wild-type cells and $n = 95$ *cin8*Δ *kip3*Δ cells; for panel D, $n = 166$ wild-type cells and $n = 166$ *cin8*Δ *kip3*Δ cells). "*n*" represents the total number of cells scored for the analysis. (E) Analysis of tubulin morphology in wild-type (SGY5001) ($n = 103$) and *cin8*Δ *kip3*Δ (SGY5089) ($n = 91$) meiosis II cells by tubulin immunostaining. Error bars represent the standard deviations from the mean values obtained from three independent experiments. A *P* value of ≥0.05 is considered nonsignificant (ns). Bars, 2 μm.

meiosis II cells of the *mam1*Δ strain in budding yeast (68) and a recombination-defective *rec8* mutant of *Schizosaccharomyces pombe* (69), where the common responsible factor is delayed nuclear separation.

Kip1 degradation is delayed in *cin8*Δ *kip3*Δ cells. In *cin8*Δ *kip3*Δ cells, although delayed, spindle elongation occurs, and we believe that Kip1 executes this function in a protracted way. In mitosis, Kip1 is degraded during the onset of anaphase by Cdc20 (34). To investigate if Kip1 becomes more stable in the absence of Cin8 and Kip3, we compared the Kip1 levels between wild-type and *cin8*Δ *kip3*Δ cells during different stages of meiosis by immunoblotting (Fig. 9A and B). Given the difference in the paces

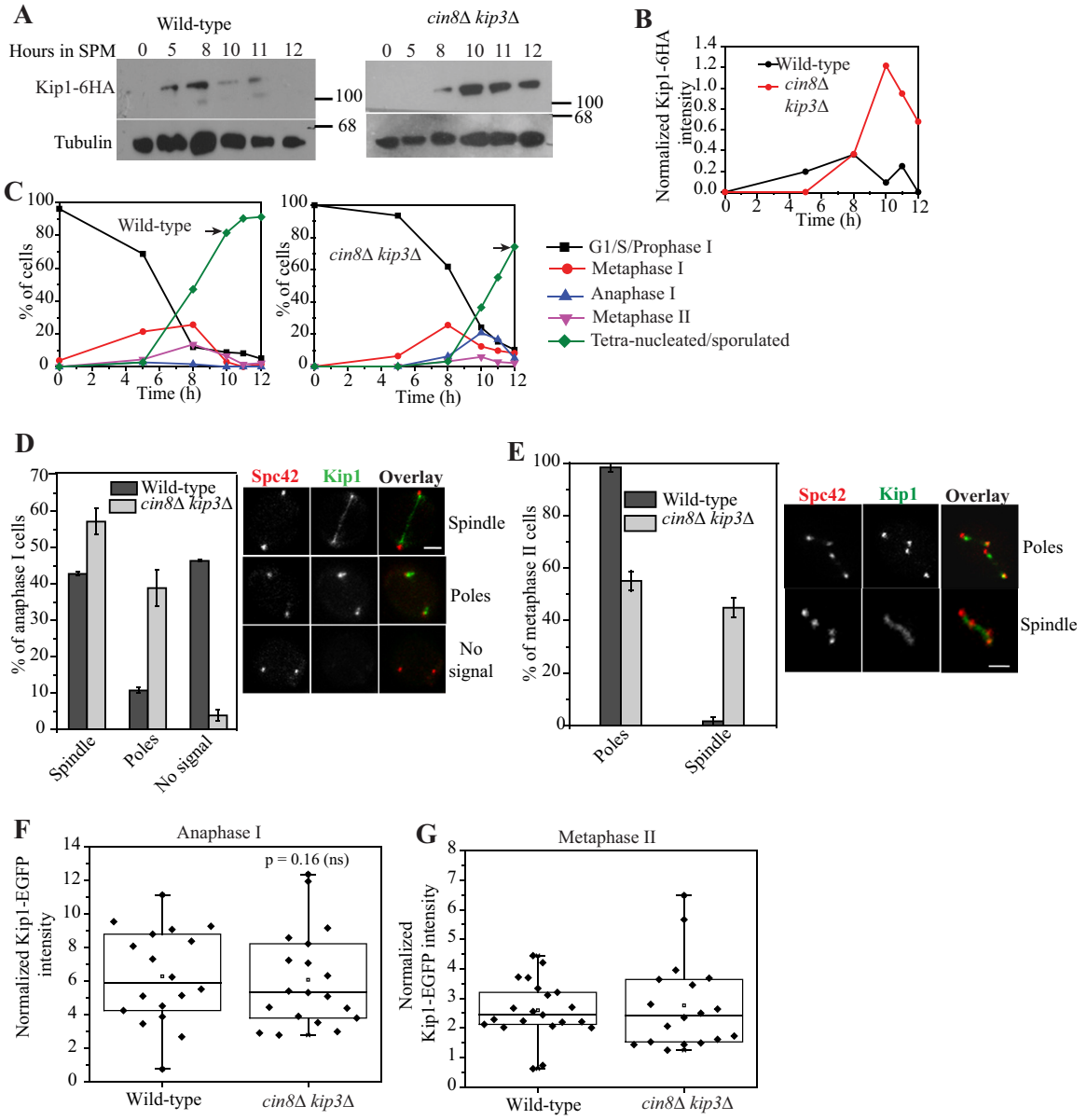

FIG 9 Increased stability of Kip1 in *cin8*Δ *kip3*Δ cells during meiosis. (A) Wild-type (SGY5539) and *cin8*Δ *kip3*Δ (SGY5540) cells harboring Kip1-6HA were induced for synchronized meiosis and analyzed for the levels of Kip1-6HA at the indicated time points during meiotic progression. Tubulin was used as a loading control. (B) Densitometric analysis of Kip1-6HA bands obtained in panel A after normalization with the respective tubulin bands using ImageJ software. (C) Percentages of prophase I, metaphase I, anaphase I, metaphase II, and anaphase II/sporulated cells determined by tubulin immunostaining of wild-type and *cin8*Δ *kip3*Δ cells at the time points utilized for Kip1-6HA detection in panels A and B ($n \geq 90$ cells for each time point). The arrow indicates a reference time point for comparison between wild-type and *cin8*Δ *kip3*Δ cells. (D and E) Localization of Kip1-EGFP in wild-type (SGY5051) and *cin8*Δ *kip3*Δ (SGY5561) cells during anaphase I (wild-type cells, $n = 56$; *cin8*Δ *kip3*Δ cells, $n = 97$) (D) and metaphase II (wild-type cells, $n = 47$; *cin8*Δ *kip3*Δ cells, $n = 165$) (E). The stage of a meiotic cell was determined by the number of and distance between the SPBs. "*n*" represents the number of cells analyzed for the assay. (F and G) Dot plots of Kip1-EGFP intensities in wild-type and *cin8*Δ *kip3*Δ cells during anaphase I (F) and metaphase II (G). Each signal intensity value was normalized to the background and Spc42-mCherry intensity values. Error bars represent the standard deviations from the mean values obtained from three independent experiments. A *P* value of ≥0.05 was considered nonsignificant (ns). Bars, 2 μm.

of the cell cycle, the 10-h stage of wild type cells was considered equivalent to the 12-h stage of *cin8*Δ *kip3*Δ cells, as the percentages of tetranucleated cells observed were almost similar (approximately 82% in wild-type and 74% in *cin8*Δ *kip3*Δ cells) (Fig. 9C). As expected, Kip1 was found to be stable for a longer duration in *cin8*Δ *kip3*Δ than in wild-type cells (Fig. 9A and B). To further examine this, we monitored the localization of Kip1 in wild-type and *cin8*Δ *kip3*Δ cells undergoing meiosis with live-cell imaging.

Stages were judged on the basis of the number of SPBs and the distance between two SPBs. In wild-type anaphase I cells, Kip1 was localized either along the spindle (42%) or near the poles (12%), while in 46% of cells, Kip1 was absent, suggesting that it is degraded toward the end of meiosis I. In contrast, Kip1 was absent in only 4% of anaphase I *cin8*Δ *kip3*Δ cells (Fig. 9D). In metaphase II, while almost 100% of wild-type cells showed a polar localization of Kip1, almost 45% of *cin8*Δ *kip3*Δ cells exhibited a single spindle-like localization spanning the 4 SPBs, suggesting that Kip1 degradation is deferred in the latter cells (Fig. 9E). However, overall, the Kip1 level was not altered, as determined by comparing Kip1-EGFP intensities between wild-type and *cin8*Δ *kip3*Δ cells at anaphase I and metaphase II (Fig. 9F and G). For intensity measurements within anaphase I cells, only spindle-localized Kip1-EGP intensities were compared between the wild type and the mutant. These results indicate that in the absence of Cin8 and Kip3, spindle elongation can still be possible, perhaps through positive regulation of Kip1 function. From the above-described localization and immunoblot studies, we propose that in the absence of a spindle localization of Cin8 and Kip3, Kip1 exhibits a greater distribution along the spindle, which may result in delayed degradation of this protein.

The tension generated by microtubule-mediated force drives efficient Rec8 removal. From the above-described results, it is evident that in the absence of both Cin8 and Kip3, Rec8 is not efficiently removed from chromatin, and this condition perhaps leads to chromosome breakage during meiosis II. What could be the reason for Rec8 retention when Cin8 and Kip3 are not present? We argue that in *cin8*Δ *kip3*Δ cells, due to the absence of microtubule cross-linking and depolymerization activities, there is inadequate microtubule-based pulling force acting on the cohesin between the sisters during meiosis I and meiosis II. Given this, we hypothesize that the generation of tension on cohesin is perhaps a novel determinant for efficient Rec8 removal. If this is true, then the generation of microtubule force in *cin8*Δ *kip3*Δ cells can rescue Rec8 cleavage and, therefore, chromosome integrity and spore viability. To test this, we expressed in these cells a phosphodeficient allele of *CIN8* (Cin8-3A) that is retained on the spindle and can generate force for an extended period or a phosphomimic allele of *CIN8* (Cin8-3D) that fails to bind to the microtubule and create force and thus exhibits a diffuse nuclear localization (31). The spindle localization of Cin8-3A but the diffuse localization of Cin8-3D in anaphase I cells confirmed their modes of action (Fig. 10A). Remarkably, in the chromosome segregation assay with homozygous CenV-GFP, we observed a drop in the percentage of tetranucleates harboring $>$4 GFP dots, a readout of chromosome breakage, in *cin8*Δ *kip3*Δ Cin8-3A cells (15%) compared to *cin8*Δ *kip3*Δ cells (29%) (type IV) (Fig. 10B). There is no significant difference in the patterns of chromosome segregation observed among the *cin8*Δ, *cin8*Δ *cin8-3A*, and *cin8*Δ *cin8-3D* mutants, suggesting that *CIN8* phosphomutants by themselves do not exhibit any additional defects (Fig. 10B). In accordance with this, the spore viability obtained for *cin8*Δ *kip3*Δ cells (approximately 16%) was ameliorated to a great extent upon the expression of Cin8-3A (approximately 48%) (Fig. 10C). These results suggest that the microtubule binding ability of Cin8-3A can partially mitigate the defects found in *cin8*Δ *kip3*Δ cells. The observed rescue effect is specific to the ability of Cin8-3A to bind to the microtubule, as *cin8*Δ *kip3*Δ cells expressing Cin8-3D showed phenotypes similar to those of *cin8*Δ *kip3*Δ cells alone (Fig. 10B and C). These results indicate that the tension generated by Cin8 and Kip3 collectively via the microtubule perhaps creates a signal for efficient cleavage and subsequent removal of Rec8.

To further test whether tension is an additional factor required for cohesin removal in meiosis, we monitored Rec8 localization after mimicking the conditions of loss of tension by two distinct approaches. During meiosis I, the tension between the homologs and on the cohesin is generated as the bipolar pulling force by the microtubule is opposed by chiasmata formed between the homologs and the cohesion formed between the sister chromatids. We inhibited chiasma formation by deleting *SPO11*, examined Rec8 localization, and compared it with the above-described results (Fig. 6A to D and Fig. 11A). Nuclear Rec8 localization was observed in around 92% of *spo11*Δ

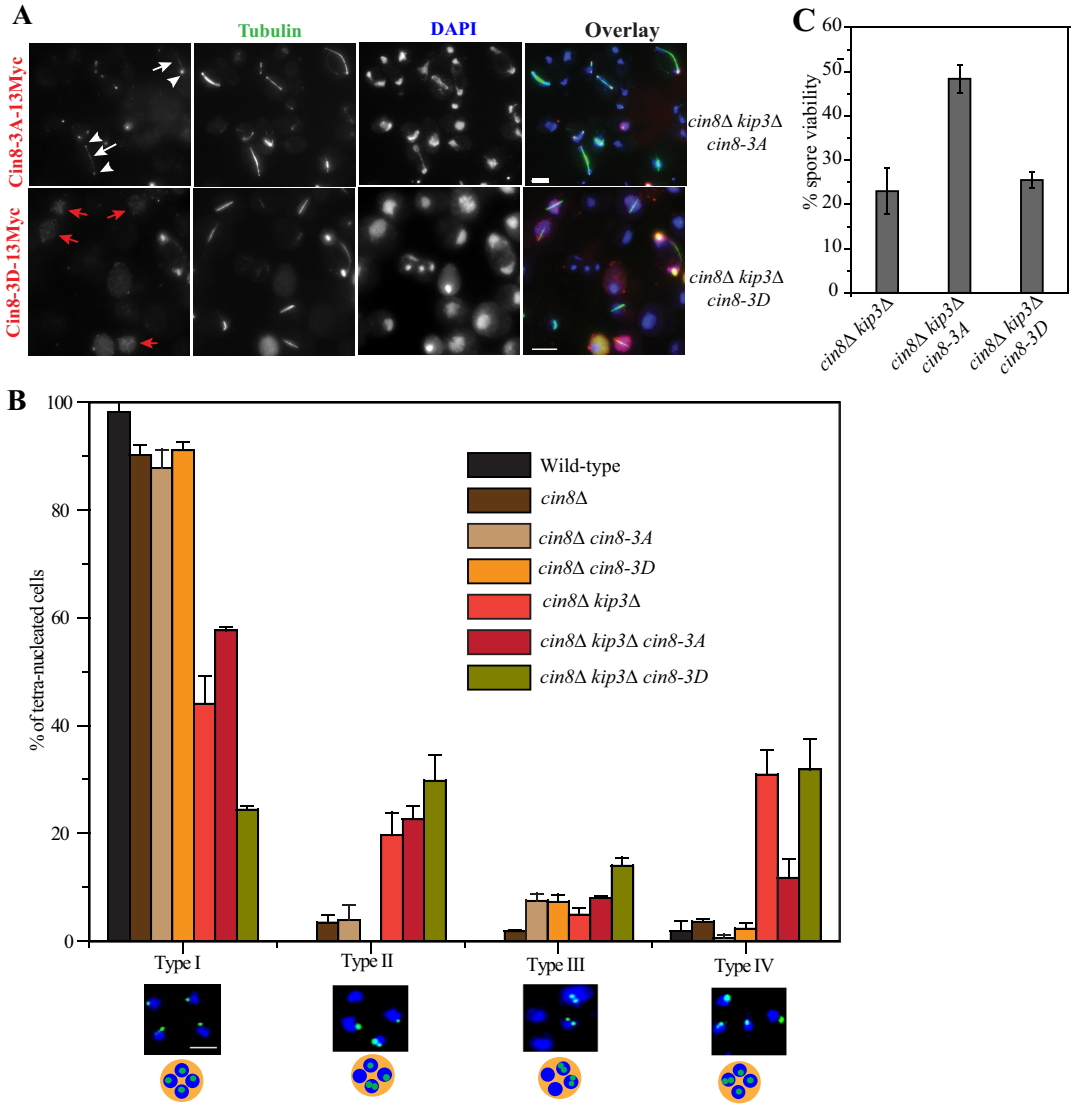

FIG 10 The absence of microtubule cross-linking activity of Cin8 is partly responsible for the defect observed in the *cin8*Δ *kip3*Δ mutant. (A) *cin8*Δ *kip3*Δ *cin8-3A–13MYC* (SGY5546) and *cin8*Δ *kip3*Δ *cin8-3D–13MYC* (SGY5547) cells expressing phosphodeficient or phosphomimic alleles of *CIN8*, respectively, were examined during meiosis for the localization of the corresponding mutant proteins with respect to the spindle. While Cin8-3A–13Myc was detected along the long spindles (white arrows) and at the poles (arrowheads), Cin8-3D–13Myc was observed as diffuse nuclear signals (red arrows). Bars, 5 μm. (B) Homozygous CenV-GFP segregation in tetranucleated cells of the wild-type (SGY5001), *cin8*Δ (SGY315), *cin8*Δ *cin8-3A–13MYC* (SGY5715), *cin8*Δ *cin8-3D–13MYC* (SGY5716), and *cin8*Δ *kip3*Δ (SGY5089) strains and the two strains used in panel A. More than 80 tetranucleates were counted for each strain. The frequency of tetranucleates with supernumerary GFP dots (type IV) was reduced in cells expressing Cin8-3A, which can bind and cross-link the microtubules. Bar, 2 μm. (C) Percentages of spore viability in the above-mentioned strains. More than 70 tetrads were dissected for each strain. Error bars represent the standard deviations from the mean values obtained from three independent experiments.

anaphase I cells, which was far greater than that observed in *cin8*Δ *kip3*Δ (65%) or in wild-type (36%) cells (Fig. 6A to C and Fig. 11A), suggesting that loss of tension indeed resists efficient cohesin removal. However, as *spo11*Δ cells proceeded to meiosis II, the Rec8 staining pattern in metaphase II became similar to that of wild-type cells. This was expected since the *spo11*Δ strain can alleviate tension only during meiosis I. In another approach to investigate the role of tension in Rec8 removal, we depolymerized microtubules using benomyl (see Materials and Methods) in cells depleted for the spindle assembly checkpoint protein Mad2 using the *CLB2* promoter so that the cells could proceed through meiosis (70). We treated the cells with benomyl after 5.5 h of meiotic release when most of the cells had passed the prophase I stage (Fig. 11B). In the

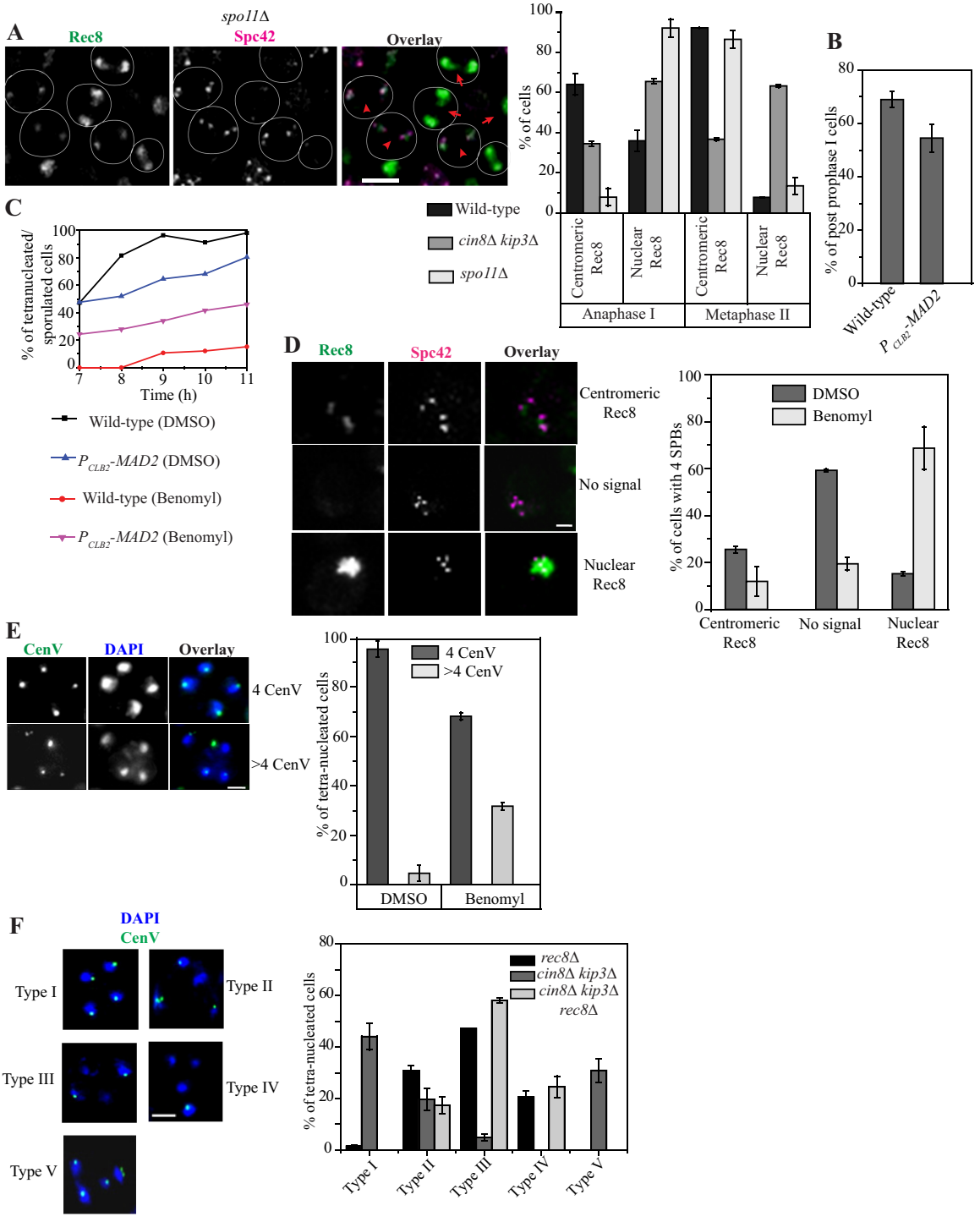

FIG 11 Tension is indispensable for the timely removal of Rec8, and deletion of *REC8* suppresses the formation of supernumerary centromeric foci in *cin8*Δ *kip3*Δ cells during meiosis. (A) Localization of Rec8-EGFP in *spo11*Δ (SGY5610) cells ($n = 220$) harboring Spc42-CFP in the anaphase I and metaphase II stages with respect to wild-type and *cin8*Δ *kip3*Δ cells, as shown in Fig. 6C and D. Representative images of *spo11*Δ cells are shown on the left, whereas those of wild-type and *cin8*Δ *kip3*Δ cells are shown in Fig. 6A and B, respectively. Based on the distribution of Rec8 staining, cells were categorized as having centromeric or nuclear Rec8, as shown by arrowheads or arrows, respectively, in the representative images. (B and C) Mad2 depletion relieves cell cycle arrest caused by microtubule disruption. Wild-type (SGY5557) and P_{CLB2}-*MAD2* (SGY5628) cells harboring Rec8-EGFP and Spc42-CFP were released into synchronized meiosis. The progression of the cells through meiosis before or after the addition of benomyl was analyzed by tubulin immunostaining and DAPI staining. (B) Percentages of cells that had progressed beyond prophase I following 5.5 h of meiotic release into drug-free medium. (C) Each meiotic culture was either mock treated (dimethyl sulfoxide [DMSO]) or treated with benomyl, and percentages of tetranucleated/sporulated cells at the indicated time points were determined. (D) Localization of Rec8-EGFP in Mad2-depleted cells harboring P_{CLB2}-*MAD2* (SGY5628) in the presence or absence of benomyl. Cells showing 4 SPBs marked by Spc42-CFP were scored for centromeric, nuclear, or no signals of Rec8. (E) P_{CLB2}-*MAD2* cells harboring homozygous CenV-GFP (SGY3248) were analyzed for the

(Continued on next page)

absence of Mad2, benomyl-treated cells were able to go through meiosis I and meiosis II although not as efficiently as mock-treated cells (Fig. 11C). Due to the absence of microtubules, as SPB separation was improper, we were unable to distinguish between metaphase I and anaphase I cells, and therefore, only the cells with 4 SPBs were analyzed. We observed that a notable population (69%) of cells harbored robust nuclear Rec8 staining in the benomyl-treated culture but no or minimal centromeric Rec8 staining in the mock-treated culture (Fig. 11D). This suggests that the removal of microtubules by benomyl reduces tension and that this in turn perturbs Rec8 cleavage. Consequently, it is expected that benomyl-treated cells harboring homozygous CenV-GFP would cause chromosome breakage during meiosis II and show supernumerary GFP foci. Although DAPI segregation in the presence of a sublethal concentration of benomyl was not as efficient as that of the mock-treated culture, we observed ~32% tetranucleated cells with supernumerary GFP foci in the presence of the drug, which was a meager 5% under unperturbed conditions (Fig. 11E). The two above-described investigations indicate that a reduction of tension can cause inefficient cohesin removal, and we suggest that this condition eventually leads to chromosome breakage, as observed in *cin8*Δ *kip3*Δ cells.

If the retention of Rec8 is responsible for chromosome breakage in *cin8*Δ *kip3*Δ cells, then the removal of Rec8 in these cells should alleviate the defect. To examine this, we deleted *REC8* in the wild-type and *cin8*Δ *kip3*Δ strains harboring homozygous CenV-GFP. Since meiosis is severely compromised in the absence of Rec8 (71), we observed a much smaller population of tetranucleates in *rec8*Δ or in *cin8*Δ *kip3*Δ *rec8*Δ cells. Due to the high rate of chromosome nondisjunction in the absence of cohesin, the percentage of tetranucleates with GFP dots in all four nuclei was negligible (approximately 1%) (type I) (Fig. 11F); instead, we observed a predominant population of tetranucleates with GFP dots in 2 nuclei in *rec8*Δ and *cin8*Δ *kip3*Δ *rec8*Δ cells (47% and 58%, respectively) (type III), while the remaining population contained GFP dots either in three of the four nuclei (31% and 17% of *rec8*Δ and *cin8*Δ *kip3*Δ *rec8*Δ cells, respectively) (type II) or in only one of the four nuclei (21% and 25% of *rec8*Δ and *cin8*Δ *kip3*Δ *rec8*Δ cells, respectively) (type IV). This gross chromosome missegregation was also evident from the asymmetric DAPI staining observed in the tetranucleated cells. However, as we expected, none of the triple mutant cells exhibited >4 CenV-GFP dots, indicating that defective cohesin removal in *cin8*Δ *kip3*Δ cells is indeed responsible for chromosome breakage, which is also depicted in our model (Fig. 12).

DISCUSSION

Faithful chromosome segregation relies on the coordinated interaction between the microtubule and chromosomes. The molecular motors profoundly influence this interaction not only by ensuring the proper attachment of the kinetochores to microtubules but also by temporally and spatially regulating the microtubule spindle. Roles of motor proteins in the context of mitotic chromosome segregation have been described in several studies (9, 14, 43, 46). However, given the differences in the patterns of chromosome movement between mitosis and meiosis, including two-time chromosome segregation with concomitant assembly, extension, and disassembly of the spindle in meiosis, it is intriguing to investigate the functions of these motors in meiosis. In this work, we analyzed the functions of three microtubule plus-end-directed kinesin motors in meiosis.

Loss of Cin8 perturbs homolog pairing and homolog disjunction. Analysis of the single-motor mutants revealed that the loss of Cin8 affects meiosis more than the loss

FIG 11 Legend (Continued)
segregation of CenV-GFP at the tetranucleated stage following microtubule depolymerization by benomyl. For panels D and E, approximately 120 to 150 cells were analyzed from benomyl-treated or untreated culture, and the drug or DMSO was added following 5.5 h of meiotic induction. (F) Analysis of CenV-GFP-marked homolog segregation in the tetranucleates of *rec8*Δ (SGY5667) ($n = 142$) and *cin8*Δ *kip3*Δ *rec8*Δ (SGY5670) ($n = 74$) cells along with the *cin8*Δ *kip3*Δ data shown in Fig. 4A. "*n*" represents the total number of tetranucleates scored for chromosome segregation. Error bars represent the standard deviations from the mean values obtained from three independent experiments. Bar, 2 μm.

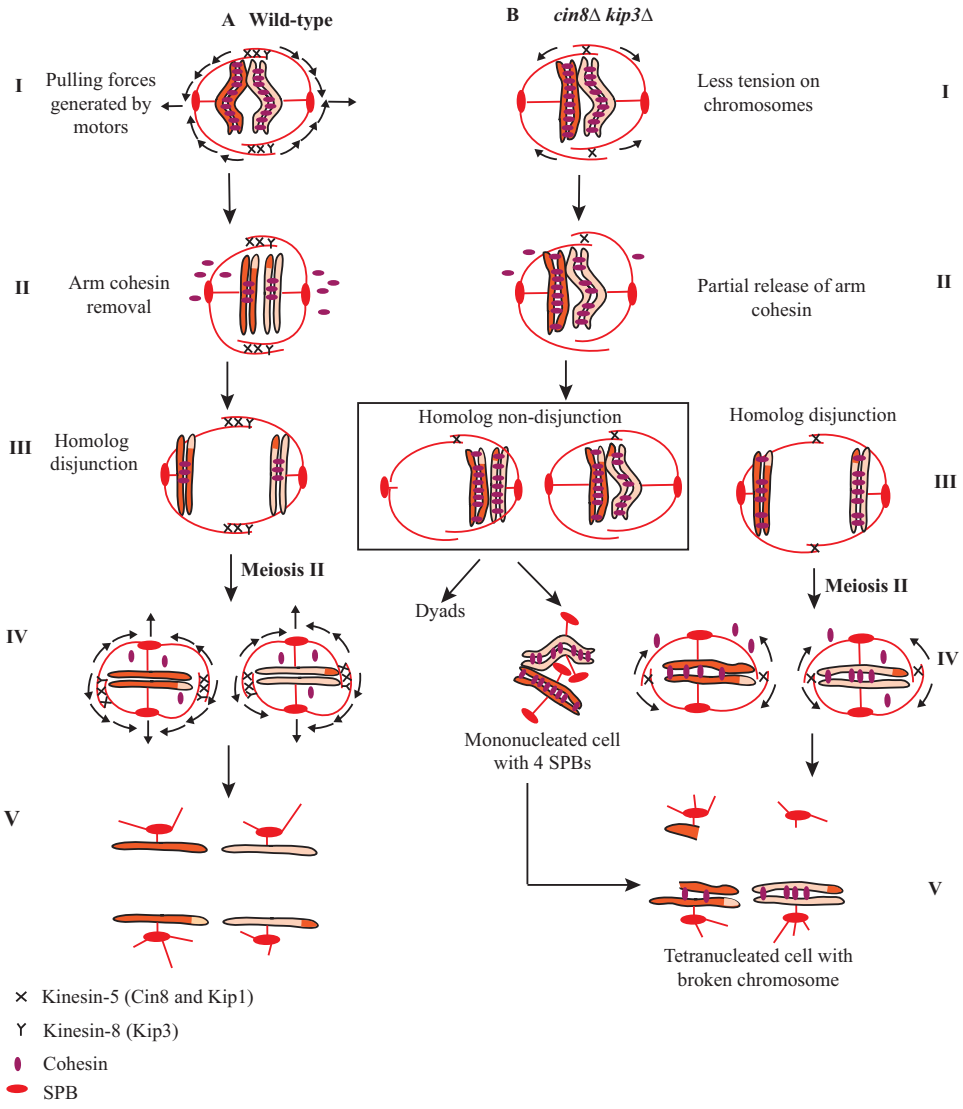

FIG 12 A possible mechanism responsible for chromosome breakage in *cin8*Δ *kip3*Δ cells. The model shows meiotic chromosome segregation in wild-type (A) and *cin8*Δ *kip3*Δ (B) cells. (I) Due to the absence of Cin8 and Kip3, the transduction of pulling force on the chromosomes by only Kip1 through sliding of the antiparallel microtubules is less in the double mutant than in the wild type. This causes a lack of tension on the cohesin, perturbing their removal. (III) The persistence of cohesin resists chiasma resolution, which, along with weak kinetochore-microtubule attachment in the *cin8*Δ *kip3*Δ mutant, results in homolog nondisjunction. These cells, after a transient delay at anaphase I, either form dyads or enter into meiosis II, showing mononucleates with 4 SPBs, perhaps due to structural blockage in disjoining chromatids, which can subsequently produce tetranucleates with broken chromosomes. (IV and V) However, in some cells, homolog disjunction occurs but with persistent cohesin (IV), which results in chromosome breakage when the cells enter meiosis II (V).

of either Kip1 or Kip3 (Fig. 1). At early meiosis, Cin8 appears to promote homolog pairing and, consequently, homolog disjunction (Fig. 2C to E). In homolog pairing, it is required that each homolog locate each other, which requires the functions of the cytoskeleton and the motors that are believed to facilitate pairing by enhancing the search rate. The function of the dynein motors with the help of the nuclear envelope-spanning SUN/KASH proteins in homolog pairing has been demonstrated in *Caenorhabditis elegans* (72, 73). In *S. pombe*, the dynein motors drive the "horsetail nuclear movement" that facilitates homolog pairing (74). In *S. cerevisiae*, the rapid prophase movements (RPMs) of chromosomes in meiosis I are believed to occur via actin and nuclear envelope motor proteins, including Mps3-Ndj1-Csm4, through interactions with telomeres (75–77). While RPMs and telomere-led movements of the chromosomes

promote homolog pairing, it is plausible that the nuclear kinesins may facilitate RPMs, or they may function in pairing independently. However, the former possibility is unlikely since no interaction among the nuclear envelope proteins and the kinesin motors has been demonstrated. With better microtubule cross-linking activity than the kinesin-8 motor (Kip3), the kinesin-5 motors (Cin8/Kip1) may have a greater role in the movement of one homolog than the other during the search for the pairing partner. The fact that we observed a more significant effect of Cin8 than of Kip1 on homolog pairing and, for that matter, on meiosis (Fig. 2C), despite both proteins belonging to the kinesin-5 family, is not surprising since it has been demonstrated that in mitosis, Cin8 plays a larger role than Kip1 in chromosome segregation (78). This is perhaps due to structural differences between these two proteins (23, 79).

Cin8 and Kip3 together are essential for timely exit from meiosis I and completion of meiosis II. Our analysis revealed that *cin8*Δ *kip3*Δ cells share the phenotypes of the FEAR mutants, which include a delay in spindle elongation and disassembly and the generation of dyads (Fig. 1Bii and iii and Fig. 3B). We believe that this happens in FEAR mutants because Cin8 dephosphorylation by FEAR pathway-released Cdc14 is essential for maintaining Cin8 at the spindle (7). Due to the lack of Cdc14 in the FEAR mutants, the phosphorylated form of Cin8 mediated by Cdk1 is enriched, which dissociates Cin8 from the spindle (31). Therefore, the spindle phenotypes observed for the FEAR mutants of meiotic cells resemble those of cells devoid of both Cin8 and Kip3. Notably, the *cin8*Δ mutant alone does not show a FEAR-like phenotype, indicating that the Kip3 function is parallel to that of Cin8, at least at the spindle, and its function might be similarly modulated by the absence of Cdc14. Although Kip3 function has not been reported to be regulated by Cdc14, in a screen using a yeast proteomic library, Kip3 was identified as one of the Cdk1 substrates (80). Given that Cdc14 is known to undo most of the Cdk1-mediated phosphorylations and that in *S. pombe*, one of the kinesin-8 members, Klp-6, is a substrate of the Cdc14 homolog Clp1 (81), it is possible that Cdc14 regulates Kip3 function in *S. cerevisiae*. In addition, similar to the FEAR mutants, *cin8*Δ *kip3*Δ cells mostly showed reductional segregation in two spores of the dyads. However, some cells completed meiosis II and produced tetranucleates but with dire consequences, as discussed below.

Improper cohesin removal in *cin8*Δ *kip3*Δ cells causes chromosome breakage in meiosis. The finding of >4 CenV-GFP foci in homozygously GFP-marked *cin8*Δ *kip3*Δ cells specifically in meiosis but not in mitosis was surprising (Fig. 3E and F; see also Fig. S2B at http://www.bio.iitb.ac.in/~santanu/wp-content/uploads/2020/05/Supplementary_file-final.pdf). Further analysis revealed that this happens due to chromosome breakage in cells that attempt to complete meiosis II (Fig. 4C). Unexpectedly, our investigations suggest that this breakage is due to the improper removal of cohesin from chromatin during both the metaphase I-to-anaphase I and metaphase II-to-anaphase II transitions (Fig. 6 and Fig. 7A to D). We believe that the anaphase I delay in *cin8*Δ *kip3*Δ cells, besides the lack of sliding of the antiparallel microtubules, is also due to the inefficient removal of cohesin from the arm regions.

Since in *cin8*Δ *kip3*Δ cells, we observed the uncoupling of Pds1 degradation from Rec8 removal (Fig. 7A to D), it is reasonable to propose that in meiosis, efficient Rec8 cleavage perhaps requires an additional factor besides the release of separase.

Microtubule based tension: a novel determinant to cleave Rec8- but not Mcd1-cohesin? It is important to address why Rec8 removal is compromised in the absence of Cin8 and Kip3 together. Both Cin8 and Kip3 localize at the kinetochore, where Kip3 is a part of the core kinetochore and is involved in kinetochore-microtubule attachment (13). On the other hand, the lack of Cin8 and Kip3 together, but not individually, causes a reduced transient separation of the sister kinetochores compared to the wild type in preanaphase mitotic cells (13), and we noticed that the metaphase-to-anaphase transition is delayed (see Fig. S1B at the URL mentioned above). These results suggest that Cin8 and Kip3 together are involved in force generation on the chromosomes toward the opposite spindle poles, which is consistent with the fact that these motors have microtubule cross-linking (19, 20,

38, 82) and depolymerase (28, 37, 38) activities. Therefore, in *cin8*Δ *kip3*Δ meiotic cells, the homologs and, thus, the sisters are not under tension in meiosis I and meiosis II, respectively. We propose a model (Fig. 12) where the efficient cleavage of Rec8 in both meioses I and II requires the homologs and the sisters, respectively, to be under tension. In support of this, in a phosphodeficient Cin8 mutant that remains bound to the spindle for a longer duration and can generate force, Rec8 removal is supposedly better, and hence, we observed less chromosome breakage and improved spore viability, the opposite of which was found in the case of a phosphomimic mutant that fails to bind to the spindle and generate force (Fig. 10B and C). To reconfirm our tension model of Rec8 cleavage, we created tensionless conditions by removing either chiasmata (*SPO11*) or microtubules in a Mad2-depleted strain and observed defective Rec8 removal under both conditions (Fig. 11A and D). Importantly, we failed to observe any perturbation of Mcd1 removal in *cin8*Δ *kip3*Δ cells (Fig. 7E), and we believe that this is why the cells perform better in mitosis (see Fig. S1D and E at the URL mentioned above). To address how tension might drive Rec8 but not Mcd1 cleavage, we reason that tension may by some means promote the phosphorylation of Rec8, and previous studies have shown that phosphorylation of Rec8, but not Mcd1, is indispensable for cohesin cleavage (4, 83, 84). Tension can influence the maintenance of certain proteins on chromatin responsible for Rec8 phosphorylation, or as a direct effect on the cohesin, it may expose the Rec8 sites for phosphorylation. Alternatively, tension may facilitate phosphorylated Rec8 amenable to cleavage by separase. It is possible that in *cin8*Δ *kip3*Δ cells, the spindle assembly checkpoint becomes activated because of a loss of tension and faulty kinetochore-microtubule attachment, which can keep APC inactivated and resist cohesin cleavage. However, we believe that this is unlikely as we observed that Pds1 degradation occurred in the double mutant at a normal pace of the cell cycle (Fig. 7B and D). To explain why a tension-based mechanism has evolved to sensitize cohesin removal in meiosis, it can be argued that in this cell cycle, unlike in mitosis, chiasmata are formed, and the removal of arm cohesin is required for their resolution. During resolution of chiasmata, the "terminalization" of the crossover point that occurs due to pulling of the homologs might subject arm cohesin to tension, which perhaps signals their removal. However, how the prolonged retention of cohesin with reduced tension acting on the chromosomes (due to the absence of Cin8 and Kip3) can eventually lead to chromosome breakage is not clear from our study. We observed that in *cin8*Δ *kip3*Δ cells, spindle disassembly is delayed (stretched category) (Fig. 8C), and Kip1 activity is protracted (Fig. 9). Additionally, the loss of these proteins can potentially cause abnormally extended kinetochores-microtubules since they also possess microtubule depolymerase activity (28, 37, 38). It is plausible that when these conditions together prevail over an extended period of time spanning two rounds of spindle assembly/disassembly and chromosome movement in meiosis, an imbalance of force is generated on the chromosomes, causing them to break. Although tension is known to cause a reorientation of the unipolar-attached chromosome and resumption of the cell cycle from arrest (85), here, we report for the first time the requirement of tension for the efficient removal of cohesin in meiosis and the importance of kinesin-5 and kinesin-8 motors in promoting this event and, thus, maintaining chromosome integrity. Given that meiosis and the functions of kinesins are conserved across eukaryotes, it would be tempting to investigate if an attenuation of motor functions could be one of the reasons for the generation of aneuploid gametes that occurs at an alarming rate during human gametogenesis.

MATERIALS AND METHODS

Yeast strains and media. All the strains used in this study were of the SK1 background. A list of strains and plasmids with their genotypes can be found in Table S1 at http://www.bio.iitb.ac.in/~santanu/wp-content/uploads/2020/05/Supplementary_file-final.pdf. The plasmids utilized for C-terminal protein tagging and deletion of a gene were obtained from Euroscarf and were PCR based (86). Transformation of the cells with the PCR cassettes was performed as mentioned previously (87). In the case of selection

of the cells on dropout medium along with the antibiotic G418, the medium was used as described previously (88), where instead of ammonium sulfate, monosodium glutamate was used to restore the sensitivity to G418. For metaphase I and prophase I arrest, P_{CLB2} and P_{GAL1} constructs were used to shuffle the endogenous promoters of *CDC20* and *NDT80*, respectively, as described previously (4, 89). For chromosome segregation assays, chromosome V and chromosome III were marked with GFP by integrating repeats of *tet* operators at 1.4 kb and *lac* operators at 22 kb away from the centromeres, respectively, in cells expressing TetR-GFP and LacI-GFP, respectively (90, 91).

Fluorescence microscopy. For live-cell imaging, 1 ml of the culture at an optical density at 600 nm (OD_{600}) of 1 was fixed with formaldehyde (final concentration, 5%) for 5 to 10 min. The pellet was washed two times with 0.1 M phosphate buffer (pH 7.5). For DAPI staining, after fixation of the sample with formaldehyde, the pellet was washed once with 50% ethanol and then resuspended in DAPI at a final concentration of 1 μg/ml. The image was acquired with z-stacking (spacing of 0.5 μm) using a Zeiss AxioObserver Z1 inverted microscope (63×, 1.4-numerical-aperture [NA] objective). Processing and merging of images were done using AxioVs40 V 4.8.2.0 software. The exposure time was set according to the fluorescence signal and was kept constant among the samples used for comparison (mainly, it was 1.5 s for EGFP, CFP, and mCherry fluorophore excitation). In order to avoid bleed-through of the intense Spc42-CFP signal in the GFP channel, a Zeiss confocal laser scanning microscope (LSM 780) equipped with a 32-array GaAsP detector was used. Images were acquired using Zeiss Zen 2012 software.

Image analysis. Images were generated by merging the planes projecting maximum intensity and further analyzed. The quantification of the fluorescence intensity of the images, acquired using a Zeiss AxioObserver Z1 microscope, was performed using ImageJ software (92). A region of interest covering the fluorescence signal was defined, and the integrated intensity of that region was estimated, following background reduction, by averaging the integrated intensities of three random nonfluorescent areas multiplied by the area of the fluorescent signal region. Estimation of the number of Rad52 or Rec8 foci per chromosome spread was performed using an automatic spot detection algorithm (Imaris3D reconstitution software), keeping the threshold limit constant for all the images.

Growth conditions and meiotic induction. Before meiotic induction, the cells were patched onto YPG (1% yeast extract, 2% peptone, 2% glycerol) to restrain the growth of petite colonies and then transferred to presporulation medium overnight. This was followed by meiotic induction in sporulation medium (0.02% raffinose, 1% potassium acetate) as described previously (93, 94).

In order to prevent the loss of the centromeric plasmid containing a mutated open reading frame (ORF) of *CIN8*, in the presporulation medium (PSP2) used for the meiosis synchronization, instead of yeast extract-potassium acetate (YPA) medium, selective medium (synthetic complete media without uracil) supplemented with 0.1% yeast extract was used (95, 96).

For mitotic synchronization, cells were arrested at G_1 using α-factor at a concentration of 5 μg/ml in cells at an OD_{600} of 0.3 (97, 98). After 3 h, when >90% of cells exhibited shmoo formation, the cells were washed and released into fresh YPD medium.

For enhancing the expression of LacI-GFP that is under the control of the *HIS3* promoter, 3-aminotriazole was added at a final concentration of 20 mM to sporulation medium.

Unlike mitosis, disruption of microtubules before or during meiotic S phase causes cells to arrest at G_1 or G_2 phase, respectively (99). Therefore, for microtubule depolymerization in meiosis, the cells were treated with benomyl at a concentration of 60 μg/ml after 5.5 h of meiotic induction, when most of the cells passed through S phase. Stages of the cell cycle and microtubule morphology before and after drug treatment were determined by tubulin immunofluorescence. In order to avoid spindle checkpoint-mediated arrest in the absence of microtubules, Mad2 was depleted in meiosis using the *CLB2* promoter (70).

Comet assay. A comet assay was performed as described previously (100). After meiotic induction in SPM for 8 h, 1 ml of the sporulating culture at a concentration of 10^7 cells per ml was harvested. Cells were then resuspended in buffer (1 M sorbitol, 25 mM KH_2PO_4, 50 mM β-mercaptoethanol [β-ME]) containing Zymolyase 20T (20 mg/ml; MP Biomedicals). The pH of the buffer was adjusted to 6.5 using NaOH. The cells were then incubated for 1/2 h for making spheroplasts. Spheroplasted cells were then mixed with 1.5% low-melting-point (LMP) agarose and spread immediately onto a glass slide precoated with 0.5% normal-melting-point (NMP) agarose. Slides were placed on ice for the agarose to solidify, in which the embedded cells formed cavities in the gel. Subsequently, the slides were submerged in lysing buffer (30 mM NaOH, 1 M NaCl, 0.05% sodium dodecyl sulfate, 50 mM EDTA, 10 mM Tris-HCl [pH 10]) for 20 min at 4°C. Following lysis of the spheroplasts, the cavities formed by the spheroplasted cells contained only high-molecular-weight DNA, while the other biomolecules diffused out. The slides were then placed into electrophoresis buffer (30 mM NaOH, 10 mM EDTA, 10 mM Tris-HCl [pH 10]) at 4°C for 20 min for the unwinding of the DNA, which was followed by electrophoresis for 20 min at 0.7 V/cm. Upon application of an electric current of 300 mA at 24 V, the fragmented DNA, named the "tail," moved toward the anode (positive electrode), while the compact mass of DNA remained in the cavity, giving a "comet"-like appearance on the gel. For each comet, the head is the mass of supercoiled DNA. Only if there is a DNA break is supercoiling released. The loose ends extend toward the anode (+) during electrophoresis, giving a tail-like appearance against the immobile compact mass of DNA. Following this, the slides were incubated in neutralization buffer (10 mM Tris-HCl [pH 7.4]) at room temperature for 10 min. The slides were incubated in 76% and 96% ethanol for 10 min each at room temperature. The slides were then incubated with a solution containing ethidium bromide (10 μg/ml) for 5 min and observed using an epifluorescence microscope (excitation filter, 546 nm; emission filter, 575 nm). Wild-type cells treated with 10 mM H_2O_2

were used as positive controls. We used a method to calculate the percentage of DNA in the tail as described previously by Braafladt et al. (56), using the formula % DNA in tail = $100 \times I_t/(I_h + I_t)$, where I_t is the total tail intensity and I_h is the total head intensity.

Immunostaining. Immunostaining was performed as described previously (94). Cells from the meiotic culture were harvested and fixed with 5% formaldehyde. Spheroplasts were made using Zymolyase and placed onto a polylysine-coated slide. The spheroplasts were permeabilized by Triton X-100 or methanol-acetone and then incubated with primary followed by secondary antibodies. DAPI (4′,6-diamidino-2-phenylindole) at a concentration of 1 μg/ml in 0.1 M phosphate buffer was used to stain the DNA. Primary antibodies, including rat antitubulin (catalog number MCA78G; Serotec) and mouse anti-Myc (catalog number 11667149001; Roche), were used at dilutions of 1:5,000 and 1:200, respectively. The secondary antibodies used, obtained from Jackson, were tetramethyl rhodamine isothiocyanate (TRITC)-labeled goat anti-rat (catalog number 115-485-166), Alexa Fluor 488-labeled goat anti-rat (catalog number 112-545-167), and TRITC-labeled goat anti-mouse (catalog number 115-025-166) antibodies at a dilution of 1:200.

Chromosome spread. The protocol for chromosome spread formation was performed as described previously (94, 101). Two milliliters of a meiotic culture was spheroplasted using Zymolyase 20T (10 mg/ml) for 1 h with 1.42 M β-ME. The reaction was stopped by the addition of 200 μl of stop solution (0.1 M morpholineethanesulfonic acid [MES], 1 mM EDTA, 0.5 mM $MgCl_2$, 1 M sorbitol [pH 6.4]). Spheroplasted cells were fixed on acid-washed slides with a paraformaldehyde solution (4% paraformaldehyde and 3.4% sucrose with 2 drops of NaOH to dissolve the paraformaldehyde), followed by the addition of 1% Lipsol to burst the cells. The slides were kept drying overnight at room temperature after homogenously smearing the spheroplasts on the slide. The next day, the slides were washed with 2 ml of 0.4% Photoflow-200 (Kodak), followed by washing in phosphate-buffered saline (PBS) for 10 min. Before the addition of primary antibodies, 100 μl of blocking solution (5% skim milk) was added to the slide for 30 min. Primary antibodies were diluted in PBS supplemented with 0.1% BSA (bovine serum albumin). Primary antibodies used were rabbit anti-Zip1 (catalog number SC 33733; Santa Cruz Biotechnology) (1:100), mouse antihemagglutinin (anti-HA) (catalog number MMS-101P; Covance) (1:200), and mouse anti-GFP (catalog number 11814460001; Roche) (1:200). The slides were coated with 100 μl of primary antibody for 1 h, followed by washing with PBS three times with a 5-min incubation each time. A similar treatment with secondary antibody was performed. Secondary antibodies from Jackson, TRITC-labeled goat anti-rat and Alexa Fluor 488-labeled goat anti-mouse (catalog number 115-485-166) antibodies, were used at a dilution of 1:200. Chromatin was stained using DAPI.

Immunoblotting and its quantification. Whole-cell proteins were extracted by NaOH treatment as described previously (102), with some modifications. Cells from 10 ml of the culture at an OD_{600} of 1 were pelleted down and treated with 0.1 N NaOH for 30 min. After alkaline treatment, pelleted cells were resuspended in electrophoresis sample buffer (2% SDS, 10% glycerol, 80 mM Tris [pH 6.8], 2% bromophenol blue, 100 mM dithiothreitol) (104) and boiled for 5 min at 100°C. The supernatant obtained after centrifugation was used for immunoblotting. Primary rabbit anti-Myc antibody (catalog number ab9106; Abcam) was used at a dilution of 1:5,000 in a 1:20 mixture of Tris-buffered saline plus Tween (TBST)–5% skim milk. Horseradish peroxidase (HRP)-conjugated secondary antibodies (Jackson) used for detection were goat anti-mouse (catalog number 115-035-166) (1:5,000), goat anti-rabbit (catalog number 111-035-003) (1:10,000), and goat anti-rat (catalog number 112-035-167) (1:10,000) antibodies. Blots were developed using ECL reagents (catalog number 170-5060; Bio-Rad Laboratories). The intensities of the bands at different time points were quantified using ImageJ software. The ratio of the protein bands to the loading control band was used for comparison between the wild-type and mutant strains.

RNA extraction and cDNA synthesis. Total RNA was extracted from the meiotic cell culture at an OD_{600} of 1.5 to 2 ($\sim 1.5 \times 10^7$ cells) using TRIzol reagent and a PureLink RNA minikit (Ambion Life Technologies). The cell pellet was resuspended in TRIzol, and cell lysis was done using diethyl pyrocarbonate (DEPC)-treated sterile 0.5-mm glass beads. The rest of the protocol was performed according to the instructions provided by the supplier (PureLink RNA minikit). RNA was eluted in DEPC (Sigma-Aldrich Chemicals Pvt. Ltd.)-treated sterile water. DNase treatment was done at 37°C for 10 min using RNase-free DNase I (Thermo Fisher Scientific) in the buffer supplied with the enzyme. The DNase was inactivated by heating at 65°C for 10 min. To ensure the absence of DNA impurity, endpoint PCR was performed with the same primers as the ones used for RT-qPCR.

cDNA synthesis was done using an iScript cDNA synthesis kit (Bio-Rad Laboratories Inc., USA) as instructed by the supplier.

RT-qPCR and data analysis. All the quantitative PCR (qPCR) experiments were performed using the CFX96 Touch real-time PCR detection system (Bio-Rad Laboratories Inc., USA). We used two reference genes, *TDH3* and *CDC19*, as internal controls to normalize the expression level of the gene of interest, *REC8*. The fold change in mRNA expression was calculated using the "$\Delta\Delta C_T$" method (103). The change in threshold cycle (ΔC_T) value was determined by normalizing the Rec8 value to the values for both reference genes for the individual strains. For $\Delta\Delta C_T$ calculation, ΔC_T values of the test samples were further normalized to the ΔC_T value of the wild type. Finally, the fold change was obtained by using the $\Delta\Delta C_T$ value determined by using the equation $2^{-\Delta\Delta C_T}$. The primers and conditions utilized for setting up RT-qPCR are shown in Tables S2 and S3, respectively, at http://www.bio.iitb.ac.in/~santanu/wp-content/uploads/2020/05/Supplementary_file-final.pdf.

ACKNOWLEDGMENTS

We are grateful to Leah Gheber for providing the *cin8* phosphomutant plasmids. We thank the central instrumental facility of IIT Bombay for the laser scanning confocal microscope.

The laboratory of S.K.G. is supported by DBT (BT/PR13909/BRB/10/1432/2015 and BT/PR20932/BRB/10/1539/2016) and CSIR [38(1457)/18/EMR-II] grants. P.M. is supported by a UGC fellowship [17-06/2012(i) EU-V], and D.T. is supported by a CSIR fellowship [09/087(0886)/2017-EMR-I].

REFERENCES

1. Buonomo SB, Rabitsch KP, Fuchs J, Gruber S, Sullivan M, Uhlmann F, Petronczki M, Toth A, Nasmyth K. 2003. Division of the nucleolus and its release of CDC14 during anaphase I depends on separase, SPO12, and SLK19. Dev Cell 4:727–739. https://doi.org/10.1016/s1534-5807(03)00129-1.
2. Marston AL, Lee BH, Amon A. 2003. The Cdc14 phosphatase and the FEAR network control meiotic spindle disassembly and chromosome segregation. Dev Cell 4:711–726. https://doi.org/10.1016/s1534-5807(03)00130-8.
3. Yellman CM, Roeder GS. 2015. Cdc14 early anaphase release, FEAR, is limited to the nucleus and dispensable for efficient mitotic exit. PLoS One 10:e0128604. https://doi.org/10.1371/journal.pone.0128604.
4. Lee BH, Amon A. 2003. Role of Polo-like kinase CDC5 in programming meiosis I chromosome segregation. Science 300:482–486. https://doi.org/10.1126/science.1081846.
5. D'Amours D, Amon A. 2004. At the interface between signaling and executing anaphase—Cdc14 and the FEAR network. Genes Dev 18:2581–2595. https://doi.org/10.1101/gad.1247304.
6. Khmelinskii A, Schiebel E. 2008. Assembling the spindle midzone in the right place at the right time. Cell Cycle 7:283–286. https://doi.org/10.4161/cc.7.3.5349.
7. Roccuzzo M, Visintin C, Tili F, Visintin R. 2015. FEAR-mediated activation of Cdc14 is the limiting step for spindle elongation and anaphase progression. Nat Cell Biol 17:251–261. https://doi.org/10.1038/ncb3105.
8. Barton NR, Goldstein LS. 1996. Going mobile: microtubule motors and chromosome segregation. Proc Natl Acad Sci U S A 93:1735–1742. https://doi.org/10.1073/pnas.93.5.1735.
9. Roof DM, Meluh PB, Rose MD. 1992. Kinesin-related proteins required for assembly of the mitotic spindle. J Cell Biol 118:95–108. https://doi.org/10.1083/jcb.118.1.95.
10. Saunders WS, Hoyt MA. 1992. Kinesin-related proteins required for structural integrity of the mitotic spindle. Cell 70:451–458. https://doi.org/10.1016/0092-8674(92)90169-d.
11. Saunders WS, Koshland D, Eshel D, Gibbons IR, Hoyt MA. 1995. Saccharomyces cerevisiae kinesin- and dynein-related proteins required for anaphase chromosome segregation. J Cell Biol 128:617–624. https://doi.org/10.1083/jcb.128.4.617.
12. Gupta ML, Jr, Carvalho P, Roof DM, Pellman D. 2006. Plus end-specific depolymerase activity of Kip3, a kinesin-8 protein, explains its role in positioning the yeast mitotic spindle. Nat Cell Biol 8:913–923. https://doi.org/10.1038/ncb1457.
13. Tytell JD, Sorger PK. 2006. Analysis of kinesin motor function at budding yeast kinetochores. J Cell Biol 172:861–874. https://doi.org/10.1083/jcb.200509101.
14. DeZwaan TM, Ellingson E, Pellman D, Roof DM. 1997. Kinesin-related KIP3 of Saccharomyces cerevisiae is required for a distinct step in nuclear migration. J Cell Biol 138:1023–1040. https://doi.org/10.1083/jcb.138.5.1023.
15. Cottingham FR, Gheber L, Miller DL, Hoyt MA. 1999. Novel roles for Saccharomyces cerevisiae mitotic spindle motors. J Cell Biol 147:335–350. https://doi.org/10.1083/jcb.147.2.335.
16. Hoyt MA, He L, Loo KK, Saunders WS. 1992. Two Saccharomyces cerevisiae kinesin-related gene products required for mitotic spindle assembly. J Cell Biol 118:109–120. https://doi.org/10.1083/jcb.118.1.109.
17. Dagenbach EM, Endow SA. 2004. A new kinesin tree. J Cell Sci 117:3–7. https://doi.org/10.1242/jcs.00875.
18. Kashina AS, Baskin RJ, Cole DG, Wedaman KP, Saxton WM, Scholey JM. 1996. A bipolar kinesin. Nature 379:270–272. https://doi.org/10.1038/379270a0.
19. Gordon DM, Roof DM. 1999. The kinesin-related protein Kip1p of Saccharomyces cerevisiae is bipolar. J Biol Chem 274:28779–28786. https://doi.org/10.1074/jbc.274.40.28779.
20. Hildebrandt ER, Gheber L, Kingsbury T, Hoyt MA. 2006. Homotetrameric form of Cin8p, a Saccharomyces cerevisiae kinesin-5 motor, is essential for its in vivo function. J Biol Chem 281:26004–26013. https://doi.org/10.1074/jbc.M604817200.
21. Mayr MI, Storch M, Howard J, Mayer TU. 2011. A non-motor microtubule binding site is essential for the high processivity and mitotic function of kinesin-8 Kif18A. PLoS One 6:e27471. https://doi.org/10.1371/journal.pone.0027471.
22. Rizk RS, Discipio KA, Proudfoot KG, Gupta ML, Jr. 2014. The kinesin-8 Kip3 scales anaphase spindle length by suppression of midzone microtubule polymerization. J Cell Biol 204:965–975. https://doi.org/10.1083/jcb.201312039.
23. Gerson-Gurwitz A, Thiede C, Movshovich N, Fridman V, Podolskaya M, Danieli T, Lakamper S, Klopfenstein DR, Schmidt CF, Gheber L. 2011. Directionality of individual kinesin-5 Cin8 motors is modulated by loop 8, ionic strength and microtubule geometry. EMBO J 30:4942–4954. https://doi.org/10.1038/emboj.2011.403.
24. Roostalu J, Hentrich C, Bieling P, Telley IA, Schiebel E, Surrey T. 2011. Directional switching of the kinesin Cin8 through motor coupling. Science 332:94–99. https://doi.org/10.1126/science.1199945.
25. Fridman V, Gerson-Gurwitz A, Shapira O, Movshovich N, Lakamper S, Schmidt CF, Gheber L. 2013. Kinesin-5 Kip1 is a bi-directional motor that stabilizes microtubules and tracks their plus-ends in vivo. J Cell Sci 126:4147–4159. https://doi.org/10.1242/jcs.125153.
26. Shapira O, Gheber L. 2016. Motile properties of the bi-directional kinesin-5 Cin8 are affected by phosphorylation in its motor domain. Sci Rep 6:25597. https://doi.org/10.1038/srep25597.
27. Shapira O, Goldstein A, Al-Bassam J, Gheber L. 2017. A potential physiological role for bi-directional motility and motor clustering of mitotic kinesin-5 Cin8 in yeast mitosis. J Cell Sci 130:725–734. https://doi.org/10.1242/jcs.195040.
28. Gardner MK, Bouck DC, Paliulis LV, Meehl JB, O'Toole ET, Haase J, Soubry A, Joglekar AP, Winey M, Salmon ED, Bloom K, Odde DJ. 2008. Chromosome congression by kinesin-5 motor-mediated disassembly of longer kinetochore microtubules. Cell 135:894–906. https://doi.org/10.1016/j.cell.2008.09.046.
29. Chee MK, Haase SB. 2010. B-cyclin/CDKs regulate mitotic spindle assembly by phosphorylating kinesins-5 in budding yeast. PLoS Genet 6:e1000935. https://doi.org/10.1371/journal.pgen.1000935.
30. Goldstein A, Siegler N, Goldman D, Judah H, Valk E, Koivomagi M, Loog M, Gheber L. 2017. Three Cdk1 sites in the kinesin-5 Cin8 catalytic domain coordinate motor localization and activity during anaphase. Cell Mol Life Sci 74:3395–3412. https://doi.org/10.1007/s00018-017-2523-z.
31. Avunie-Masala R, Movshovich N, Nissenkorn Y, Gerson-Gurwitz A, Fridman V, Koivomagi M, Loog M, Hoyt MA, Zaritsky A, Gheber L. 2011. Phospho-regulation of kinesin-5 during anaphase spindle elongation. J Cell Sci 124:873–878. https://doi.org/10.1242/jcs.077396.
32. Goldstein A, Goldman D, Valk E, Loog M, Holt LJ, Gheber L. 2018. Synthetic-evolution reveals that phosphoregulation of the mitotic kinesin-5 Cin8 is constrained. bioRxiv 312637.
33. Gordon DM, Roof DM. 2001. Degradation of the kinesin Kip1p at anaphase onset is mediated by the anaphase-promoting complex and

Cdc20p. Proc Natl Acad Sci U S A 98:12515–12520. https://doi.org/10.1073/pnas.231212498.
34. Hildebrandt ER, Hoyt MA. 2001. Cell cycle-dependent degradation of the Saccharomyces cerevisiae spindle motor Cin8p requires APC (Cdh1) and a bipartite destruction sequence. Mol Biol Cell 12:3402–3416. https://doi.org/10.1091/mbc.12.11.3402.
35. Arellano-Santoyo H, Geyer EA, Stokasimov E, Chen GY, Su X, Hancock W, Rice LM, Pellman D. 2017. A tubulin binding switch underlies Kip3/kinesin-8 depolymerase activity. Dev Cell 42:37–51. https://doi.org/10.1016/j.devcel.2017.06.011.
36. Tang NH, Toda T. 2015. Alp7/TACC recruits kinesin-8-PP1 to the Ndc80 kinetochore protein for timely mitotic progression and chromosome movement. J Cell Sci 128:354–363. https://doi.org/10.1242/jcs.160036.
37. Su X, Qiu W, Gupta ML, Jr, Pereira-Leal JB, Reck-Peterson SL, Pellman D. 2011. Mechanisms underlying the dual-mode regulation of microtubule dynamics by Kip3/kinesin-8. Mol Cell 43:751–763. https://doi.org/10.1016/j.molcel.2011.06.027.
38. Su X, Arellano-Santoyo H, Portran D, Gaillard J, Vantard M, Thery M, Pellman D. 2013. Microtubule-sliding activity of a kinesin-8 promotes spindle assembly and spindle-length control. Nat Cell Biol 15:948–957. https://doi.org/10.1038/ncb2801.
39. Hoyt MA, He L, Totis L, Saunders WS. 1993. Loss of function of Saccharomyces cerevisiae kinesin-related CIN8 and KIP1 is suppressed by KAR3 motor domain mutations. Genetics 135:35–44.
40. Bascom-Slack CA, Dawson DS. 1997. The yeast motor protein, Kar3p, is essential for meiosis I. J Cell Biol 139:459–467. https://doi.org/10.1083/jcb.139.2.459.
41. Shanks RM, Kamieniecki RJ, Dawson DS. 2001. The Kar3-interacting protein Cik1p plays a critical role in passage through meiosis I in Saccharomyces cerevisiae. Genetics 159:939–951.
42. Saunders W, Hornack D, Lengyel V, Deng C. 1997. The Saccharomyces cerevisiae kinesin-related motor Kar3p acts at preanaphase spindle poles to limit the number and length of cytoplasmic microtubules. J Cell Biol 137:417–431. https://doi.org/10.1083/jcb.137.2.417.
43. Hildebrandt ER, Hoyt MA. 2000. Mitotic motors in Saccharomyces cerevisiae. Biochim Biophys Acta 1496:99–116. https://doi.org/10.1016/s0167-4889(00)00012-4.
44. Mayer ML, Pot I, Chang M, Xu H, Aneliunas V, Kwok T, Newitt R, Aebersold R, Boone C, Brown GW, Hieter P. 2004. Identification of protein complexes required for efficient sister chromatid cohesion. Mol Biol Cell 15:1736–1745. https://doi.org/10.1091/mbc.e03-08-0619.
45. Gladstone MN, Obeso D, Chuong H, Dawson DS. 2009. The synaptonemal complex protein Zip1 promotes bi-orientation of centromeres at meiosis I. PLoS Genet 5:e1000771. https://doi.org/10.1371/journal.pgen.1000771.
46. Winey M, Bloom K. 2012. Mitotic spindle form and function. Genetics 190:1197–1224. https://doi.org/10.1534/genetics.111.128710.
47. Kapitein LC, Peterman EJ, Kwok BH, Kim JH, Kapoor TM, Schmidt CF. 2005. The bipolar mitotic kinesin Eg5 moves on both microtubules that it crosslinks. Nature 435:114–118. https://doi.org/10.1038/nature03503.
48. Kamieniecki RJ, Shanks RM, Dawson DS. 2000. Slk19p is necessary to prevent separation of sister chromatids in meiosis I. Curr Biol 10:1182–1190. https://doi.org/10.1016/s0960-9822(00)00723-5.
49. Zeng X, Saunders WS. 2000. The Saccharomyces cerevisiae centromere protein Slk19p is required for two successive divisions during meiosis. Genetics 155:577–587.
50. Rock JM, Amon A. 2009. The FEAR network. Curr Biol 19:R1063–R1068. https://doi.org/10.1016/j.cub.2009.10.002.
51. Stegmeier F, Visintin R, Amon A. 2002. Separase, polo kinase, the kinetochore protein Slk19, and Spo12 function in a network that controls Cdc14 localization during early anaphase. Cell 108:207–220. https://doi.org/10.1016/S0092-8674(02)00618-9.
52. Queralt E, Lehane C, Novak B, Uhlmann F. 2006. Downregulation of PP2A (Cdc55) phosphatase by separase initiates mitotic exit in budding yeast. Cell 125:719–732. https://doi.org/10.1016/j.cell.2006.03.038.
53. Tanaka K, Kitamura E, Kitamura Y, Tanaka TU. 2007. Molecular mechanisms of microtubule-dependent kinetochore transport toward spindle poles. J Cell Biol 178:269–281. https://doi.org/10.1083/jcb.200702141.
54. Ostling O, Johanson KJ. 1984. Microelectrophoretic study of radiation-induced DNA damages in individual mammalian cells. Biochem Biophys Res Commun 123:291–298. https://doi.org/10.1016/0006-291x(84)90411-x.
55. Miloshev G, Mihaylov I, Anachkova B. 2002. Application of the single cell gel electrophoresis on yeast cells. Mutat Res 513:69–74. https://doi.org/10.1016/S1383-5718(01)00286-8.
56. Braafladt S, Reipa V, Atha DH. 2016. The comet assay: automated imaging methods for improved analysis and reproducibility. Sci Rep 6:32162. https://doi.org/10.1038/srep32162.
57. Resnick MA, Martin P. 1976. The repair of double-strand breaks in the nuclear DNA of Saccharomyces cerevisiae and its genetic control. Mol Gen Genet 143:119–129. https://doi.org/10.1007/bf00266917.
58. Malone RE, Esposito RE. 1980. The RAD52 gene is required for homothallic interconversion of mating types and spontaneous mitotic recombination in yeast. Proc Natl Acad Sci U S A 77:503–507. https://doi.org/10.1073/pnas.77.1.503.
59. Orr-Weaver TL, Szostak JW, Rothstein RJ. 1981. Yeast transformation: a model system for the study of recombination. Proc Natl Acad Sci U S A 78:6354–6358. https://doi.org/10.1073/pnas.78.10.6354.
60. Barlow JH, Rothstein R. 2009. Rad52 recruitment is DNA replication independent and regulated by Cdc28 and the Mec1 kinase. EMBO J 28:1121–1130. https://doi.org/10.1038/emboj.2009.43.
61. Gasior SL, Wong AK, Kora Y, Shinohara A, Bishop DK. 1998. Rad52 associates with RPA and functions with rad55 and rad57 to assemble meiotic recombination complexes. Genes Dev 12:2208–2221. https://doi.org/10.1101/gad.12.14.2208.
62. Lisby M, Rothstein R, Mortensen UH. 2001. Rad52 forms DNA repair and recombination centers during S phase. Proc Natl Acad Sci U S A 98:8276–8282. https://doi.org/10.1073/pnas.121006298.
63. Agarwal M, Mehta G, Ghosh SK. 2015. Role of Ctf3 and COMA subcomplexes in meiosis: implication in maintaining Cse4 at the centromere and numeric spindle poles. Biochim Biophys Acta 1853:671–684. https://doi.org/10.1016/j.bbamcr.2014.12.032.
64. Lin W, Wang M, Jin H, Yu H-G. 2011. Cohesin plays a dual role in gene regulation and sister-chromatid cohesion during meiosis in Saccharomyces cerevisiae. Genetics 187:1041–1051. https://doi.org/10.1534/genetics.110.122358.
65. Buonomo SB, Clyne RK, Fuchs J, Loidl J, Uhlmann F, Nasmyth K. 2000. Disjunction of homologous chromosomes in meiosis I depends on proteolytic cleavage of the meiotic cohesin Rec8 by separin. Cell 103:387–398. https://doi.org/10.1016/s0092-8674(00)00131-8.
66. Challa K, Fajish VG, Shinohara M, Klein F, Gasser SM, Shinohara A. 2019. Meiosis-specific prophase-like pathway controls cleavage-independent release of cohesin by Wapl phosphorylation. PLoS Genet 15:e1007851. https://doi.org/10.1371/journal.pgen.1007851.
67. Klapholz S, Waddell CS, Esposito RE. 1985. The role of the SPO11 gene in meiotic recombination in yeast. Genetics 110:187–216.
68. Toth A, Rabitsch KP, Galova M, Schleiffer A, Buonomo SB, Nasmyth K. 2000. Functional genomics identifies monopolin: a kinetochore protein required for segregation of homologs during meiosis I. Cell 103:1155–1168. https://doi.org/10.1016/s0092-8674(00)00217-8.
69. Yamamoto A, Kitamura K, Hihara D, Hirose Y, Katsuyama S, Hiraoka Y. 2008. Spindle checkpoint activation at meiosis I advances anaphase II onset via meiosis-specific APC/C regulation. J Cell Biol 182:277–288. https://doi.org/10.1083/jcb.200802053.
70. Jin H, Guacci V, Yu H-G. 2009. Pds5 is required for homologue pairing and inhibits synapsis of sister chromatids during yeast meiosis. J Cell Biol 186:713–725. https://doi.org/10.1083/jcb.200810107.
71. Klein F, Mahr P, Galova M, Buonomo SB, Michaelis C, Nairz K, Nasmyth K. 1999. A central role for cohesins in sister chromatid cohesion, formation of axial elements, and recombination during yeast meiosis. Cell 98:91–103. https://doi.org/10.1016/S0092-8674(00)80609-1.
72. Penkner AM, Fridkin A, Gloggnitzer J, Baudrimont A, Machacek T, Woglar A, Csaszar E, Pasierbek P, Ammerer G, Gruenbaum Y, Jantsch V. 2009. Meiotic chromosome homology search involves modifications of the nuclear envelope protein Matefin/SUN-1. Cell 139:920–933. https://doi.org/10.1016/j.cell.2009.10.045.
73. Sato A, Isaac B, Phillips CM, Rillo R, Carlton PM, Wynne DJ, Kasad RA, Dernburg AF. 2009. Cytoskeletal forces span the nuclear envelope to coordinate meiotic chromosome pairing and synapsis. Cell 139:907–919. https://doi.org/10.1016/j.cell.2009.10.039.
74. Wells JL, Pryce DW, McFarlane RJ. 2006. Homologous chromosome pairing in Schizosaccharomyces pombe. Yeast 23:977–989. https://doi.org/10.1002/yea.1403.
75. Conrad MN, Lee CY, Chao G, Shinohara M, Kosaka H, Shinohara A, Conchello JA, Dresser ME. 2008. Rapid telomere movement in meiotic prophase is promoted by NDJ1, MPS3, and CSM4 and is modulated by

recombination. Cell 133:1175–1187. https://doi.org/10.1016/j.cell.2008.04.047.
76. Koszul R, Kim KP, Prentiss M, Kleckner N, Kameoka S. 2008. Meiotic chromosomes move by linkage to dynamic actin cables with transduction of force through the nuclear envelope. Cell 133:1188–1201. https://doi.org/10.1016/j.cell.2008.04.050.
77. Wanat JJ, Kim KP, Koszul R, Zanders S, Weiner B, Kleckner N, Alani E. 2008. Csm4, in collaboration with Ndj1, mediates telomere-led chromosome dynamics and recombination during yeast meiosis. PLoS Genet 4:e1000188. https://doi.org/10.1371/journal.pgen.1000188.
78. Geiser JR, Schott EJ, Kingsbury TJ, Cole NB, Totis LJ, Bhattacharyya G, He L, Hoyt MA. 1997. Saccharomyces cerevisiae genes required in the absence of the CIN8-encoded spindle motor act in functionally diverse mitotic pathways. Mol Biol Cell 8:1035–1050. https://doi.org/10.1091/mbc.8.6.1035.
79. Singh SK, Pandey H, Al-Bassam J, Gheber L. 2018. Bidirectional motility of kinesin-5 motor proteins: structural determinants, cumulative functions and physiological roles. Cell Mol Life Sci 75:1757–1771. https://doi.org/10.1007/s00018-018-2754-7.
80. Ubersax JA, Woodbury EL, Quang PN, Paraz M, Blethrow JD, Shah K, Shokat KM, Morgan DO. 2003. Targets of the cyclin-dependent kinase Cdk1. Nature 425:859–864. https://doi.org/10.1038/nature02062.
81. Chen X, Suhandynata RT, Sandhu R, Rockmill B, Mohibullah N, Niu H, Liang J, Lo H-C, Miller DE, Zhou H, Börner GV, Hollingsworth NM. 2015. Phosphorylation of the synaptonemal complex protein Zip1 regulates the crossover/noncrossover decision during yeast meiosis. PLoS Biol 13:e1002329. https://doi.org/10.1371/journal.pbio.1002329.
82. Voelkel-Meiman K, Cheng S-Y, Parziale M, Morehouse SJ, Feil A, Davies OR, de Muyt A, Borde V, MacQueen AJ. 2019. Crossover recombination and synapsis are linked by adjacent regions within the N terminus of the Zip1 synaptonemal complex protein. PLoS Genet 15:e1008201. https://doi.org/10.1371/journal.pgen.1008201.
83. Alexandru G, Uhlmann F, Mechtler K, Poupart MA, Nasmyth K. 2001. Phosphorylation of the cohesin subunit Scc1 by Polo/Cdc5 kinase regulates sister chromatid separation in yeast. Cell 105:459–472. https://doi.org/10.1016/s0092-8674(01)00362-2.
84. Attner MA, Miller MP, Ee L, Elkin SK, Amon A. 2013. Polo kinase Cdc5 is a central regulator of meiosis I. Proc Natl Acad Sci U S A 110:14278–14283. https://doi.org/10.1073/pnas.1311845110.
85. Nicklas RB, Koch CA. 1969. Chromosome micromanipulation. III. Spindle fiber tension and the reorientation of mal-oriented chromosomes. J Cell Biol 43:40–50. https://doi.org/10.1083/jcb.43.1.40.
86. Wach A, Brachat A, Alberti-Segui C, Rebischung C, Philippsen P. 1997. Heterologous HIS3 marker and GFP reporter modules for PCR-targeting in Saccharomyces cerevisiae. Yeast 13:1065–1075. https://doi.org/10.1002/(SICI)1097-0061(19970915)13:11<1065::AID-YEA159>3.0.CO;2-K.
87. Gietz RD, Schiestl RH. 2007. High-efficiency yeast transformation using the LiAc/SS carrier DNA/PEG method. Nat Protoc 2:31–34. https://doi.org/10.1038/nprot.2007.13.
88. Cheng TH, Chang CR, Joy P, Yablok S, Gartenberg MR. 2000. Controlling gene expression in yeast by inducible site-specific recombination. Nucleic Acids Res 28:E108. https://doi.org/10.1093/nar/28.24.e108.
89. Benjamin KR, Zhang C, Shokat KM, Herskowitz I. 2003. Control of landmark events in meiosis by the CDK Cdc28 and the meiosis-specific kinase Ime2. Genes Dev 17:1524–1539. https://doi.org/10.1101/gad.1101503.
90. Straight AF, Belmont AS, Robinett CC, Murray AW. 1996. GFP tagging of budding yeast chromosomes reveals that protein-protein interactions can mediate sister chromatid cohesion. Curr Biol 6:1599–1608. https://doi.org/10.1016/s0960-9822(02)70783-5.
91. Tanaka T, Fuchs J, Loidl J, Nasmyth K. 2000. Cohesin ensures bipolar attachment of microtubules to sister centromeres and resists their precocious separation. Nat Cell Biol 2:492–499. https://doi.org/10.1038/35019529.
92. Mittal P, Chavan A, Trakroo D, Shah S, Ghosh SK. 2019. Outer kinetochore protein Dam1 promotes centromere clustering in parallel with Slk19 in budding yeast. Chromosoma 128:133–148. https://doi.org/10.1007/s00412-019-00694-9.
93. Cha RS, Weiner BM, Keeney S, Dekker J, Kleckner N. 2000. Progression of meiotic DNA replication is modulated by interchromosomal interaction proteins, negatively by Spo11p and positively by Rec8p. Genes Dev 14:493–503.
94. Mehta GD, Agarwal M, Ghosh SK. 2014. Functional characterization of kinetochore protein, Ctf19 in meiosis I: an implication of differential impact of Ctf19 on the assembly of mitotic and meiotic kinetochores in Saccharomyces cerevisiae. Mol Microbiol 91:1179–1199. https://doi.org/10.1111/mmi.12527.
95. Roth R, Halvorson HO. 1969. Sporulation of yeast harvested during logarithmic growth. J Bacteriol 98:831–832. https://doi.org/10.1128/JB.98.2.831-832.1969.
96. Simchen G, Pinon R, Salts Y. 1972. Sporulation in Saccharomyces cerevisiae: premeiotic DNA synthesis, readiness and commitment. Exp Cell Res 75:207–218. https://doi.org/10.1016/0014-4827(72)90538-1.
97. Cui H, Ghosh SK, Jayaram M. 2009. The selfish yeast plasmid uses the nuclear motor Kip1p but not Cin8p for its localization and equal segregation. J Cell Biol 185:251–264. https://doi.org/10.1083/jcb.200810130.
98. Prajapati HK, Rizvi SM, Rathore I, Ghosh SK. 2017. Microtubule-associated proteins, Bik1 and Bim1, are required for faithful partitioning of the endogenous 2 micron plasmids in budding yeast. Mol Microbiol 103:1046–1064. https://doi.org/10.1111/mmi.13608.
99. Hochwagen A, Wrobel G, Cartron M, Demougin P, Niederhauser-Wiederkehr C, Boselli MG, Primig M, Amon A. 2005. Novel response to microtubule perturbation in meiosis. Mol Cell Biol 25:4767–4781. https://doi.org/10.1128/MCB.25.11.4767-4781.2005.
100. Oliveira R, Johansson B. 2012. Quantitative DNA damage and repair measurement with the yeast comet assay. Methods Mol Biol 920:101–109. https://doi.org/10.1007/978-1-61779-998-3_8.
101. Prajapati HK, Agarwal M, Mittal P, Ghosh SK. 2018. Evidence of Zip1 promoting sister kinetochore mono-orientation during meiosis in budding yeast. G3 (Bethesda) 8:3691–3701. https://doi.org/10.1534/g3.118.200469.
102. Kushnirov VV. 2000. Rapid and reliable protein extraction from yeast. Yeast 16:857–860. https://doi.org/10.1002/1097-0061(20000630)16:9<857::AID-YEA561>3.0.CO;2-B.
103. Livak KJ, Schmittgen TD. 2001. Analysis of relative gene expression data using real-time quantitative PCR and the $2^{-\Delta\Delta CT}$ method. Methods 25:402–408. https://doi.org/10.1006/meth.2001.1262.
104. Dunn SD. 1986. Effects of the modification of transfer buffer composition and the renaturation of proteins in gels on the recognition of proteins on Western blots by monoclonal antibodies. Anal Biochem 1:144–153. https://doi.org/10.1016/0003-2697(86)90207-1.